`Vol. 5, No. 3, pp. 262-294, (September 2024)
DOI: 10.21608/aujes.2024.287639.1235
Aswan University Journal of Environmental Studies (AUJES)
Online ISSN: 2735-4237, Print ISSN: 2735-4229
Journal homepage: https://aujes.journals.ekb.eg/ E-mail: AUJES@aswu.edu.eg
Original research

Analysis and Design of Frequency Regulation Controllers with Considering Communication Delays and Environmental Effects of Renewable Energy Microgrids

Mostafa Eid, Mokhtar Aly*, Emad A. Mohamed, Adel Fathy, Samia Heshmat

Electrical Engineering Department, Faculty of Engineering, Aswan University, Aswan 81542, Egypt

Received: 8/5/2024 Accepted: 1/8/2024

Abstract:

Recently, with the increased awareness of the harmful and environmental effects of conventional energy resources, new renewable energy sources (RESs) have proven better solutions and replacement candidates. Increasing the participation levels of RESs in electricity generation systems can relieve the effects of greenhouse gases and increased temperature of the earth. However, the inherent characteristics of RESs based generation systems are different from the conventional synchronous generator-based generation, particularly from the side of inertia support. Additionally, increased installations lead to having continuously reduced power systems' inertia. Therefore, designing proper load frequency controllers (LFCs) represents an efficient way to face the inertial problems of RESs-based modern power grid systems. The LFC systems are subjected to different communication delays, which exist in the LFC control loops and the generation commands. Therefore, this paper presents an optimized design methodology for LFC methods. The proposed design methodology presents the design of integral (I), proportional-integral (PI), and proportional-integral-derivative (PID) controllers for LFC applications. The manta-ray foraging optimizer (MRFO) algorithm is proposed for the design optimization process. Sensitivity analysis against the different communication delay locations and values is made in the paper to compare and evaluate the considered control method. Additionally, the effects of the intermittency property of RESs are considered in the design verifications and comparisons. The obtained results show the stability issues of existing communication delays and their margin values to preserve the stable operation of power grids. Additionally, the RESs fluctuations are highly affecting the frequency response and regulation of RESs-based modern power grids. The current study provides a comprehensive and generalized method for evaluating the effects of communication time delays while considering the high penetration levels of RESs. The study can be employed for better design of LFC methods and the development of highly reliable control methods for regulating the frequency in modern power grids.

Keywords: communication delays, load frequency controllers (LFCs), manta-ray foraging optimizer (MRFO) algorithm, PID controllers, renewable energy sources, sensitivity analysis.

Corresponding author*: E-mail address: mokhtar.aly@aswu.edu.eg

1. Introduction

1. 1. Overview

The imperative energy sector shift towards new-clean renewable energy sources (RESs) in the different applications of the sector is necessitated to face the resulting harmful climate change effects on the earth and human life (Aly and Rezk, 2020; Nasiri Avanaki and Sarvi, 2016; Zhong et al., 2008). Additionally, the existing limited availability of fossil fuel resources with their continuous increase in prices motivates the replacement of RESs in the energy sector as well as the transport sector. With the recent technological developments in the RESs materials and industrial processes have emerged as a competitive option with lowered levelized cost of energy (LCOE). Another factor is the widespread accessibility of RESs in different resources all over the world, such as sun, wind, oceans, etc. The vast replacements of RESs have also led to minimizing environmental impacts and the greenhouse emissions resulting from conventional energy resources (Nasirov et al., 2018).

However, the main critical challenges that face the recent advancements and installations of RESs in modern power grids are summarized as follows:

- The generated output power from RES is dependent on continuously changing environmental conditions, such as solar irradiance, operating temperature, wind speed values, etc. As an example, photovoltaic (PV) systems do not generate power at night times nor when being subjected to shading and dust effects. Hence, their output power varies throughout the day times with the normal/abnormal changes in solar irradiance and temperature. This characteristic results in having intermittent property of RESs output power. This problem represents a significant attribute of RESs due to this intermittent nature that provides output power output fluctuations. These fluctuations are reflected as frequency deviations in modern power grid systems (*Advanced Frequency Regulation Strategies in Renewable-Dominated Power Systems*, 2024).
- Furthermore, the incorporation of more RES installations and systems into power grids leads to a continual reduction in the inertia of electrical power systems compared to fossil fuel conventional power grid systems. Power system inertia serves as a crucial determinant of power grid stability and resiliency. The diminished inertia is primarily coming from the unique voltage and current output characteristics of RESs, which cannot be directly integrated into power grids. To ensure adequate voltage, current, and power quality waveforms compatible with power grids, a power electronic power conversion unit becomes essential. These power conversion units differ from conventional energy systems, relying on the use of synchronous generators with inherent inertial support, which play a vital role in preserving system stability and robustness. This property is absent in the RESs-based power grids with the employed power electronics-based conversion systems (El-Sousy et al., 2023a).
- Another source of uncertainty arises from the characteristics of contemporary connected loads, which can undergo significant and abrupt changes. Consequently, when coupled with the unpredictable generation of RES, modern power grids may experience severe instability-related problems and inadequate responses. The changes in both generations and loading demands result in having unbalanced active power and hence higher frequency fluctuations in the power grid's frequency (Bakeer et al., 2023).

1. 2. Literature Review

To address these challenges, different energy storage systems (ESSs) have become indispensable components of modern power grids to mitigate the existing fluctuations in RES generation systems (Choudhary et al., 2022). Including ESSs represents a perfect solution for storing and supplying energy based on existing fluctuations in generation and load imbalance conditions. Therefore, effective control and management algorithms are imperative to optimize the utilization of different forms of ESS technologies and to provide support to modern power grid systems' inertial response (Singh and Arya, 2023a).

The control strategies and their proper design methodologies, which have been implemented across various interconnected elements of power grids, play a pivotal role in determining the system's response, behavior, stability, efficiency, and resilience. LFCs have emerged as efficient tools for regulating the frequency response of modern power grids. Incorporating LFCs helps to consider the imbalance between generation and connected loads. LFCs also can manage variations in tie-line power and control the contributions of connected devices, whether in a centralized or distributed manner (Nour et al., 2023a; Zaid et al., 2023).

The existing literature has presented numerous control methodologies and design approaches that have been applied to various power grid structure-based case studies. These structures encompass conventional generation resources, diverse load types, interconnected RESs, ESS devices, flexible AC transmission system (FACTS) devices, and transmission line configurations (Ahmed et al., 2023). Furthermore, the chosen design methodologies for LFCs and other controllers in modern power grids significantly influence the system's response to power imbalance-related disturbances. Mathematical-based design methodologies have been widely presented in the literature. The mathematical design techniques can achieve robust system response with the closed loop systems' guaranteed gain and phase margin. However, they need very complex methods for designing them and expert control design engineers (Ahmed et al., 2022).

On the other side, the metaheuristic optimization algorithms have been presented in the literature for designing LFCs in grid systems (Nayak et al., 2023a, 2023b). With the use of recent and classical optimization techniques, optimized control parameters are determined through the proper selection of the desired objective function. In contrast to mathematically based design methodologies found in the literature, the application of metaheuristic optimization algorithms in designing LFCs for grid systems offers a straightforward process, simultaneous parameters' tuning, eliminates the need for sophisticated and complex control theories, and allows the flexible adjustments of desired power grid response through the minimization of an objective function. Normally, objective functions are implanted based on minimizing the frequency and tie-line power fluctuations (El-Sousy et al., 2023b). Some examples of applied recent optimization techniques include the modified liver-cancer optimizer algorithm (MLCA) (Noman et al., 2024), salp swarm-based algorithm (SSA) (Arya and Singh, 2024; Rangi et al., 2024), artificial hummingbird optimization algorithm (AHA) (Mohamed et al., 2023a), global neighborhood algorithm (GNA) (Choudhary et al., 2023), etc.

Numerous LFC methodologies have been proposed in the existing literature to regulate frequency in various grid/microgrid structures. Recently, there has been a recent development in advanced and intelligent control techniques for LFC, including model-based predictive controllers (MPC), adaptive neuro-fuzzy interface systems (ANFIS), artificial neural network (ANNs), deep

learning-based neural networks (DNNs), and controllers that employ fuzzy logic (FLCs) concepts (Almasoudi et al., 2023; Mohamed et al., 2023b). However, these methods need extensive training data and more complex implementations.

Moreover, some research proposals have been introduced based on using the MPC grid stabilization approach in wind energy generation turbines (Aly et al., 2023a). In another work, an ANFIS-based LFC method has been applied to multi-RES related scenarios, utilizing the ant-lion optimizations algorithm (ALO) for optimizing the LFC design process. Additionally, an ANN-based LFC scheme was introduced for solar PV-based power plants (Shabani et al., 2013). Another hybrid controller that combines FLC and the fractional order (FO) based control techniques has been presented for two interconnected microgrids featuring PV and wind power generation while employing the wild-horse optimizer (WHO) algorithm for LFC design. This method achieves a reduced overshot, shorter settling times, and an improved power system response. The marine predator-based optimizer algorithm (MPA) has been employed in combination with the FLC-based proportional-integral-derivative (PID) control. Another LFC solution has been introduced based on an FLC PID controller with sine-cosine optimization algorithms (SCA) for designing the LFC scheme. Furthermore, frequency regulation through using FOPID FLC has been achieved with the aid of differential evolution optimizer algorithms (DE). However, these methods suffer from complex design procedures, expert requirements, huge tunning data, and/or complex implementation processes (Abid et al., 2023; Salama et al., 2022; Youssef et al., 2023).

An evaluation comparing the various advanced LFC methodologies with classical ones was conducted in (El-Sousy et al., 2023b; Mohamed et al., 2023b). The study showed that advanced LFC techniques can enhance the stability of modern power grids. However, they depend on expert systems and necessitate substantial tuning data during the design phase, along with a high computational burden and powerful processors for optimization and implementation (Ray et al., 2011; Sahu et al., 2016). In contrast, classical integer order (IO) and fractional order (FO) based LFC schemes are still having research and industry interest due to their simplicity, comprehensibility, and wide applicability in the literature. They also have the advantages of the simple implementation and hardware requirements. Thence, they demonstrate superior performance applications compared with various LFC design algorithms (Aly et al., 2023b; Arora et al., 2021; El Yakine Kouba et al., 2015).

Several IO LFC schemes have been widely introduced in the literature for LFC in several single and multi-area interconnected power grid systems (Ebeed et al., 2024). The integral (I) controller represents the widely applied IO controller in LFC problems in the literature. The PI IO-based LFC has been presented in the literature to improve the performance of I-based LFC methods. Furthermore, the PID controller has been proposed in several papers for adding the derivative term to the classical PI LFC schemes. The PID-based LFC schemes have shown improved performance and control response compared with the I and PI control methods (Sahoo et al., 2023; Singh and Arya, 2023b). Optimization algorithms have been integrated with IO LFC for design optimization and to avoid complex mathematical and control theory-based design procedures. The presented optimization methods have included the Harris Hawks optimization (HHO), imperialist-competitive optimizer algorithm (ICA), artificial bee-colony optimizer (ABC), Jaya-Balloon optimizations (JBO), the Electro-Searching Optimization (ESO) algorithm with the Balloon Effects (BE), etc (Hassan et al., 2023).

Furthermore, some strategies have been introduced based on virtual inertia control (VIC) to rapidly regulate the frequency (Almasoudi et al., 2024; Nour et al., 2023b). For instance, fuel cells based on green hydrogen systems have been introduced to enhance the inertial response through the VIC of power grids. A nonlinear PI controller, optimized using the dandelion optimizer algorithm (DO), was developed for a single-area power grid. The particle swarm optimizer algorithm (PSO) was applied for designing I and PI controllers for LFC and VICs, respectively, within interconnected microgrids. The IO LFC methods stood out for their straightforward structures, reduced complexity, uncomplicated design procedures, and cost-effective implementation. However, they showed some limitations in fully mitigating grid fluctuations, sensitivity to parameter variations, and limited design flexibility (Hassan et al., 2023). Recent applications of the artificial rabbits' optimization algorithm (ARO) for control design were also highlighted, including ARO's use in designing conventional PI and PID controllers for multi-sourced microgrid systems, as well as the design of a PD-PID accelerated controller for static synchronous compensators (STATCOM) in power systems. Additionally, a Fuzzy PIDD2 controller was presented alongside the Gradient-Based Optimizer (GBO) algorithm for stabilizing combined voltage-frequency loops in two-area-based interconnected grids. However, few works in the literature have discussed the sensitivity of designed control methods against communication time delays (Bakeer et al., 2022). However, the study of communication delays in the designed control methods has not been covered in detail.

1. 3. Problem Formulation

The necessity of a communication infrastructure has been emphasized by researchers. In practical systems, various sources are typically situated at disparate geographical locations, while the controller may be positioned elsewhere. In such cases, communication systems are necessary for transmitting both sensor information and controller outputs. It is presumed that these communications occur via shared communication channels. When shared communication channels are employed, the transmission of information may entail unpredictable delays. It is asserted that, although these delays are minor, they can induce instability in the system. Consequently, it becomes imperative to assess the performance of the control scheme under the influence of uniformly distributed random communication delays, encompassing the existing delays between sensors and the controller and between the controller and various participating units. These delays are assumed to vary randomly within the range of 0.05 to 0.15 seconds, following a uniform distribution. Therefore, a sensitivity study of the stability of LFC systems is necessary against the existing time delays of communication systems. Additionally, other effects of environmental conditions on the generated RES power have to be seriously considered in the evaluations of the designed LFC methods.

1. 4. Paper Contribution

The main contributions of this paper are summarized as follows:

- This paper proposes an optimized design methodology for IO-based LFC methods for RESs-based modern power grids. The controllers considered are the I, PI, and PID LFC schemes. However, the proposed method is general and can be extended to various LFC methods.
- The manta-ray foraging optimizer (MRFO) algorithm is presented for determining the optimized control parameters. The MRFO algorithm determines all the possible control parameters optimally and simultaneously, obtaining the best parameter set.

- This paper evaluates the sensitivity analysis of the designed LFC methods against the existing communication time delays in the studied modern power grid systems. Additionally, the wide range of time delay variations is considered in this paper to determine the possible margin values for the stable operation of RESs-based grids.

The remaining parts of this paper are organized as follows: Section 2 presents the mathematical representations of various considered grid elements of the selected case study. This Section also studies the effects of environmental factors on the installed RESs and their impact on the frequency response of the studied power grid. The various considered LFC methods are presented in Section 3. The proposed MRFO-based design optimization and the design procedures are detailed in Section 4. Section 5 presents the considered modeling of communication time delays and their related considerations. The obtained results are presented in Section 6. Finally, the conclusions of the paper are given in Section 7.

2. Materials and Methods

2. 1. System Description

The diagram in Figure 1 illustrates an isolated hybrid power system comprising diverse distributed generators (DGs) (Sharma and Mishra, 2020). This system encompasses PV (Photovoltaic), WTG (Wind Turbine Generator), AE (Advanced Energy), FC (Fuel Cell), DEG (Diesel Engine Generator), BESS (Battery Energy Storage System), and FESS (Flywheel Energy Storage System). To regulate the system's frequency, a secondary integral controller is employed. Two distinct approaches for frequency regulation in such systems have been proposed in previous references, specifically, (Pan and Das, 2016; Ray et al., 2011). In (Ray et al., 2011), a decentralized controller is presented, with each participating element having its individual controller. Conversely, (Pan and Das, 2016) adopts a unified controller approach, where a single controller governs all the sources, dispatching the same control instructions to all elements. It's important to note that utilizing a single controller, as discussed in (Pan and Das, 2016), can lead to a degradation in system performance. However, (Pan and Das, 2016) also underscores the advantages of this approach, including simplified maintenance, reduced wiring complexity, and a decrease in the number of controller parameters. Consequently, in our study, we have chosen to employ a single controller despite the participation of more than one element.

Another notable distinction between the methodologies of (Pan and Das, 2016; Ray et al., 2011) lies in the use of energy-storing devices (such as batteries and flywheels) as the primary control action to address energy needs during transient periods (Ray et al., 2011), owing to their rapid response. In contrast, (Pan and Das, 2016) employs BESS and FESS even for secondary control actions. In our paper, we have followed the approach outlined in (Ray et al., 2011), utilizing BESS and FESS exclusively for primary control to ensure swift responses during transients, while preserving their stored energy by not utilizing them during steady-state operation. The various transfer functions depicted in Figure 1, as detailed in (Pan and Das, 2016; Ray et al., 2011), are briefly discussed.

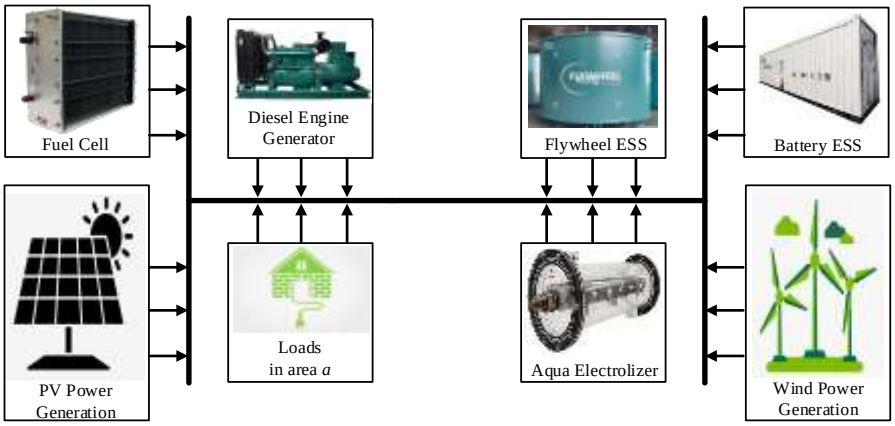

Fig. 1. Main components and structure of the studied System.

2.1. 1. PV Generation Modelling

Recently, power systems have been subjected to high penetration levels of renewable energy sources to replace conventional generation methods. In particular, the plan of the Egyptian government is to lead the renewable energy sector in the region and export renewable energy to the surrounding countries and Europe. The PV generation has received high interest due to having high irradiation levels in all the parts of Egypt, making it super competitive with other countries, in terms of the cost of generated energy.

The structure of the PV generation unit includes the PV panels, which are responsible for converting the solar irradiance into electrical energy at its terminals. It includes a DC/DC power electronic converter system, which is responsible for the extraction of maximum power from the PV source and for boosting the low voltage at the PV panel terminals into a suitable level for grid integration. In addition, it includes a DC/AC power electronic inverter system, which is responsible for the generation of AC output voltage to inject the generated power from the PV system into the utility grid system. Also, it includes some interfacing and protection devices for improving the system lifetime and for protecting the personals around the PV system.

The use of power electronic DC/AC inverters in the integration of PV power with the grid side can transfer the generated power within two-to-three-line cycles using pulse width modulations (PWM) methods. Therefore, it is suitable to employ only a first-order-based TF for the modeling of the PV system in this work. The transfer function (TF) model of PV systems is represented through using a first-order TF. The PV system TF representation is expressed as follows (El-Sousy et al., 2023a):

$$G_{PV} = \frac{K_{PV}}{T_{PV}s + 1} \quad (1)$$

where K_{PV} and T_{PV} are PV system gain, and PV system time constant. During this work, it is assumed that there is a perfect maximum power point tracking (MPPT) controller that preserves PV system operation at MPP at all times, regardless of solar irradiation changes and/or temperature changes. Thence, all the received energy from the sun is directly injected into the power grid system without reduction. This, in turn, will affect the power balance of the power system and introduce additional frequency fluctuations in the power system.

On the other side, the total generated power from the PV system is directly proportional to the solar irradiance level (φ) in addition to the operating ambient temperature. The generated power P_{PV} can be expressed as (Aly et al., 2023a):

$$P_{PV} = \eta_{PV}\, \varphi\, A_{PV}(1 - 0.005\,(T_a + 25)\,) \quad (2)$$

where, η_{PV} represents the PV panel conversion efficiency for the considered case study. Whereas A_{PV} represents the total area of the installed PV panels and subjected to the solar irradiance value (φ) from the sun in kW/m^2. The symbol T_a represents the operating point ambient temperature of the PV system. In this work, this model will be used to model the PV generated power and its dynamics as disturbances for the power grid system.

Changes and variations in solar irradiance levels result in fluctuations in PV-generated power. These fluctuations, in addition to the existing fluctuations in loading, cause unbalanced conditions between loading and generation powers, which are reflected as fluctuations in the power system's operating frequency.

2.1. 2. Wind Generation Modelling

From the wind power generation point of view, the generated wind power is highly dependent on the employed wind turbine behavior in addition to the operating wind speed of the system. The received wind power on the turbine blades makes them rotate and they hold the rotor of the generator of wind power. This rotation with the excitation field enables the generator to generate electrical power from the wind movement. The output power from the generator is converted into two series conversions from AC to DC and then the DC is converted to AC another time. This is due to the fact that the frequency of generated power from wind generation is variable based on the velocity of the wind. Then, an AC/DC rectifier stage is used to obtain a DC voltage from the variable frequency AC voltage from the generation side. Then, the second stage of DC/AC inverter system is used for the generation of controlled voltage with grid line frequency voltage waveform to make it suitable and synchronized with the power grid side system.

Also, based on using a power electronic converter structure in wind energy transition, a first-order TF will be used for the representation of wind power dynamical behavior in this work. The wind power TF can be expressed as follows (Hassan et al., 2023):

$$G_{wind} = \frac{K_{wind}}{T_{wind}\, s + 1} \quad (3)$$

where K_{wind} and T_{wind} are the model gain of wind generation, and the model time constant for the wind generation system. Also, here is assumed that there are perfect control methods to continuously achieve MPPT for all the operating points of wind power generation systems. Therefore, all the available wind power will be directly injected into the power grid system within this work. Moreover, the various expected faults and abnormal conditions with the degradation and aging of various components in the wind generation systems are neglected within this work, and hence, perfect control and operation are considered.

On the other side, the extracted wind power is a function of the wind turbine model and the operating wind speed. It can be expressed as follows (Ahmed et al., 2023):

$$P_{wind} = \frac{1}{2}\, \rho\, A_{wind}\, C_p\, v_w^3 \quad (4)$$

where ρ denotes the operating air density, A_{wind} denotes the swept area by wind turbine blades system, C_p stands for wind power coefficient, which is a function of the wind tip-speed ratio,

whereas v_w stands for the operating wind velocity. It is clear that changes of wind speed cause changes in wind-generated power by the turbine and generator systems.

2.1. 3. Distributed Generation and Storage Devices Modelling

In this paper, we will study the way to model the various installed distributed energy resources (DERs) systems in the frequency regulation study. The ESS in the power system will also be considered in this part to provide a generalized representation of the various power system elements. The considered elements in this study include the battery ESS (BESS), flywheel ESS (FESS), diesel engine generator (DEG), fuel cell (FC), and aqua electrolyzes (AE). Usually, the various DERs are represented using a first order transfer function to represent their dynamics, and hence it will be employed within this work. The system with the models and components is shown in Figure 2. The representations of the various DERS dynamics can be expressed in the following expressions (Sharma and Mishra, 2020).

For the BESS with gain K_{BESS} and time constant T_{BESS}, TF G_{BESS} is expressed as:

$$G_{BESS} = \frac{K_{BESS}}{T_{BESS}s + 1} \quad (5)$$

For the FESS with gain K_{FESS} and time constant T_{FESS}, TF G_{FESS} is expressed as:

$$G_{FESS} = \frac{K_{FESS}}{T_{FESS}s + 1} \quad (6)$$

For the FC with gain K_{FC} and time constant T_{FC}, TF G_{FC} is expressed as:

$$G_{FC} = \frac{K_{FC}}{T_{FC}s + 1} \quad (7)$$

For the AE with gain K_{BESS} and time constant T_{BESS}, TF G_{AE} is expressed as:

$$G_{AE} = \frac{K_{AE}}{T_{AE}s + 1} \quad (8)$$

For the DEG with gain K_{DEG} and time constant T_{DEG}, TF G_{DEG} is expressed as:

$$G_{DEG} = \frac{K_{DEG}}{T_{DEG}s + 1} \quad (9)$$

The use of the first-order TF is suitable for frequency regulation studies, regardless of the exhibited nonlinearities and high-order representations of the actual systems. This is because low frequency related signals are considered in frequency control. Therefore, high-order and model nonlinearities are neglected and are not considered here in the work.

2.1. 4. Power System Grid Modelling

In the balanced power operating point, the generated power from sources is equal to the consumed power at the same moment. In the current case study, the generated wind power, PV power, fuel cell power, and DEG power summation must equal the consumed power in the loads and AE power. The ESS devices can play the role of generation units during the discharging mode of operation, and the role of loading in the case of charging scenarios. The control of ESS devices is made based on the system requirement and variations in the loading behavior with respect to the generation behavior. Any power mismatches will activate the control and management algorithms to adjust the generated/stores/loading powers to cope with the current operating scenario.

The power generation and loading mismatches result in frequency deviations in the power system operating points. The amount of fluctuation is related to the amount of power mismatches, the power system operating inertia (*H*), and the power system damping (*D*). If we represent the power summation of the power generated from the controllable power sources with P_{MG}, and the connected loads P_L power, then the steady state power balance can be represented as follows (Sharma and Mishra, 2020):

$$P_L = P_{MG} + P_{PV} + P_{wind} \quad (10)$$

In case of sudden power disturbances and hence instantaneous unbalance between the generation power and loading power, the system loses its power balance condition, and frequency deviations result accordingly. The power system dynamics TF can also be represented using a first-order TF based on the values of D and H. It can be expressed as follows:

$$G_{PS} = \frac{\Delta f}{\Delta P_{MG} + dist.} = \frac{1}{2\,H\,s + D} \quad (11)$$

where Δf represents the change/deviation in the operating power system frequency. Whereas *dist.* denotes the existing power disturbance, which mainly results from the changes/unbalance of power generation/loading of the power grid system. The disturbance can be expressed as (Sharma and Mishra, 2020):

$$dist. = -\Delta P_L + \Delta P_{PV} + \Delta P_{wind} \quad (12)$$

The employed power system model parameters are summarized in Table. I for the work done in this paper. The LFC is responsible for preserving the frequency changes/deviations within the predefined power grid limits by the codes.

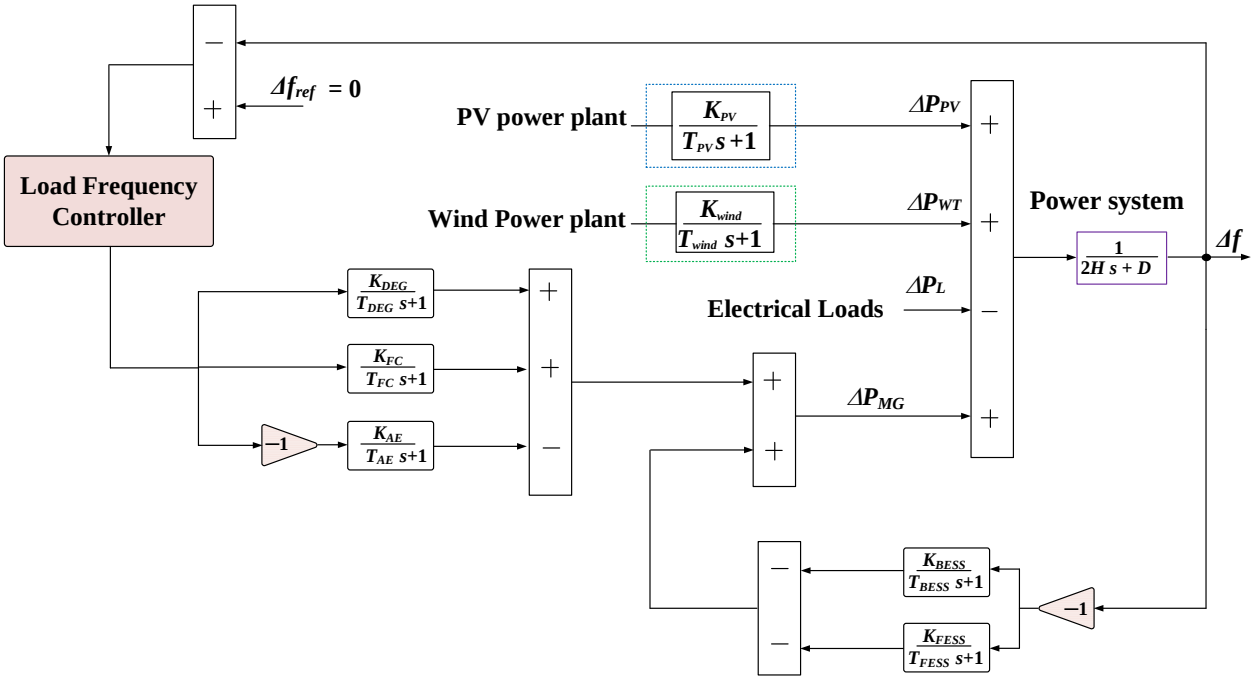

Fig. 2. Complete elements' models for the selected case study.

Table I. System parameters of he studied microgrid case

Element	Parameter	Value
PV system	K_{PV}	1.0
	T_{PV}	1.3 s
Wind system	K_{wind}	1.0
	T_{wind}	1.5 s
FC system	K_{FC}	0.01
	T_{FC}	4.0 s
DEG system	K_{DEG}	0.003
	T_{DEG}	2.0 s
BESS system	K_{BESS}	-0.003
	T_{BESS}	0.1 s
FESS system	K_{FESS}	-0.01
	T_{FESS}	0.1 s
AE system	K_{AE}	0.002
	T_{AE}	0.5 s
Power grid system	H	0.2 s
	D	0.03

2. 2. Frequency Regulation Controllers

IO-based control methods have found wide industrial applications in literature. Their performance and simple implementation, in addition to the simple design procedures, are the main advantages of IO control algorithms. Particularly, IO-based controllers are preferred solutions in LFC applications and the regulation process of operating power system frequency. There are several versions of IO-based LFC algorithms that have been developed in the literature for several case studies, including the cases of single-area power systems and multi-area power systems. In addition, they were applied to perform the LFC functionality and/or the virtual inertia control methods.

The IO-based integrator IO-I controller has been widely used in LFC applications. The IO-I possesses a single tunable parameter in its design. It is represented by the integral part gain (K_I). The diagram representing the IO-I LFC method is shown in Figure 3. The mathematical representation of the IO-I controller is expressed as:

$$C_{IO-I}(s) = \frac{Y(s)}{E(s)} = \frac{K_I}{s} \tag{13}$$

where, $C_{IO-I}(s)$ denotes the controller TF of the IO-I LFC method. Whereas $Y(s)$ is the output signal of the IO-I controller and $E(s)$ is the input error signal to the IO-I controller (here it is the ACE signal).

On the other side, the IO-based proportional-integral (IO-PI) controller has been introduced to improve the IO-I controller with the inclusion of an additional P term, which can improve the tracking speed for the reference and, hence, faster response is obtained. The IO-PI controller includes the P term gain (K_P) and the I term gain (K_I) as tunable parameters. Therefore, the IO-PI controller adds more flexibility to the LFC design. Figure 4 shows the structure of the IO-PI-based LFC system. The IO-PI controller can be mathematically expressed as:

$$C_{IO-PI}(s) = \frac{Y(s)}{E(s)} = K_P + \frac{K_I}{s} \quad (14)$$

where, $C_{IO-PI}(s)$ denotes to the controller TF of the IO-PI LFC method with ACE signal as input $E(s)$ and its output $Y(s)$ is applied to control the various generation/storage devices.

A more particular controller case study is represented through the development of the IO based proportional-integral-derivative IO-PID controller. It includes three different tunable controller parameters compared to the two tunable in IO-PI and the single tunable parameter in the IO-I controller. Therefore, better tracking with improved steady-state performance has been proven features of the IO-PID controller. The IO-PID controller includes the P term gain (K_P), the I term gain (K_I), and the D term gain (K_D) as tunable parameters of the controller design process. Therefore, the IO-PID controller has the best control flexibility compared to the IO-I LFC and the IO-PI LFC methods. Figure 5 shows the structure of the IO-PID-based LFC system. The IO-PID controller can be mathematically expressed as:

$$C_{IO-PID}(s) = \frac{Y(s)}{E(s)} = K_P + \frac{K_I}{s} + K_D\, s \quad (15)$$

where, $C_{IO-PID}(s)$ stands for the TF representation of the IO-PID LFC method using ACE signal as input $E(s)$ to the controller. Whereas the controller output signal $Y(s)$ is used to control the active power of each of the controllable sources in the studied system.

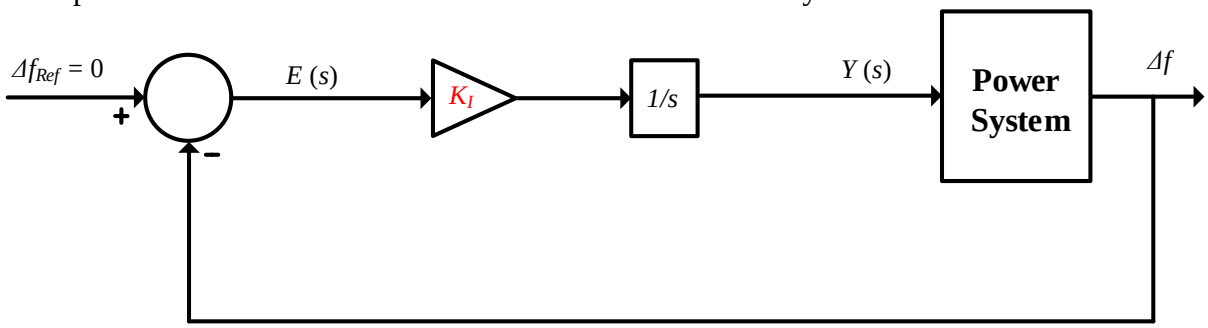

Fig. 3. LFC based on IO-I Controller

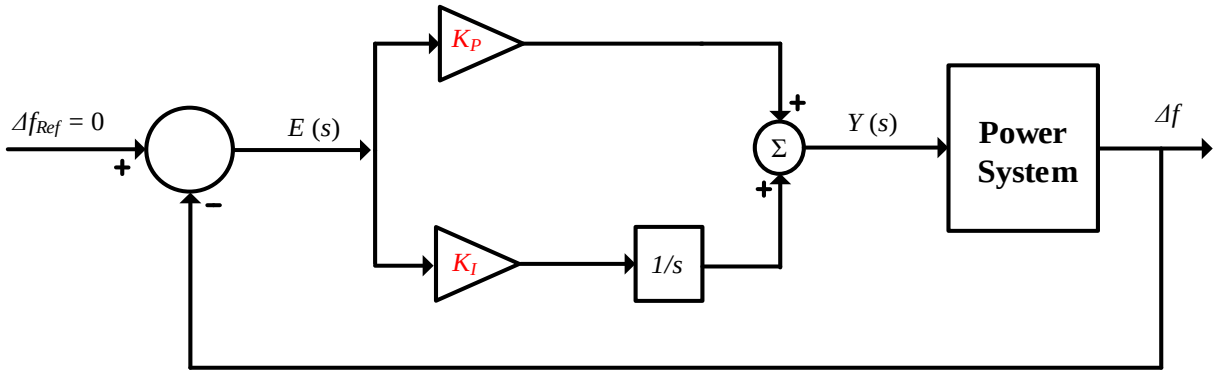

Fig. 4. LFC based on IO-PI Controller

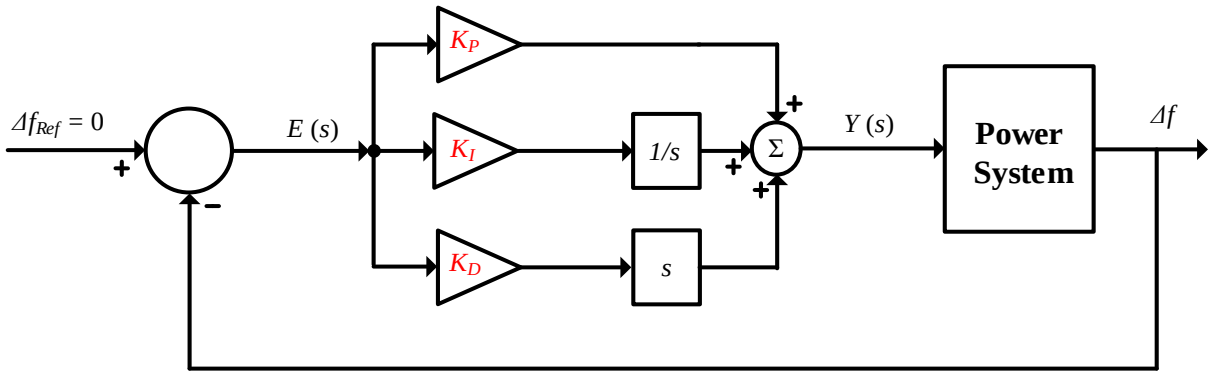

Fig. 5. LFC based on IO-PID Controller

In literature, there are several developed IO controllers for LFC studies. However, the previously presented three IO LFC methods will be considered in this work due to their generality and the focus of the paper. The focus will be on the evaluation of the three controllers while considering the different time delay models and representations of the modern power grids systems.

2. 3. Controllers Design and Optimization

2.3. 1. The MRFO Algorithm Description

Here, the MRFO optimization algorithm is employed for designing the various studied controllers in this work. The MRFO represents a metaheuristic optimization algorithm, which is related to the foraging strategies that are followed by the manta rays during the catching processes of the prey (Zhao et al., 2020). The MRFO algorithm is mainly consisting of three main foraging processes, represented by the chain process, cyclone process, and the somersault process for foraging. Firstly, the chain related process for foraging can be mathematically represented as following (Zhao et al., 2020):

$$x_i^{t+1} = \begin{cases} x_i^t + r.(x_{best}^t - x_i^t) + \omega_1.(x_{best}^t - x_i^t), i = 1 \\ x_i^t + r.(x_{i-1}^t - x_i^t) + \omega_1.(x_{best}^t - x_i^t), i = 2{:}N \end{cases} \quad (16)$$

where, x_i^t denotes to the i^{th} position of the current iteration number t and the variable x_{best}^t represents the best solutions. In addition, r stands for a randomly selected vector, N denotes to the manta rays' number, and ω_1 represents a weighting coefficient in the algorithm.

Secondly, the cyclone processes related foraging can be expressed as following (Aly and Rezk, 2021):

$$\begin{aligned} x_i^{t+1} &= x_{best} + r.(x_{i-1}^t - x_i^t) + e^{b\omega}.cos(2\pi\omega).(x_{best} - x_i^t) \\ y_i^{t+1} &= y_{best} + r.(y_{i-1}^t - y_i^t) + e^{b\omega}.cos(2\pi\omega).(y_{best} - y_i^t) \end{aligned} \quad (17)$$

where, ω represent a randomly selected number. Therefore, the cyclone process related foraging can be expressed as following (Zhao et al., 2020):

$$x_i^{t+1} = \begin{cases} x_{best} + r.(x_{best}^t - x_i^t) + \omega_2.(x_{best}^t - x_i^t), i = 1 \\ x_{best} + r.(x_{i-1}^t - x_i^t) + \omega_2.(x_{best}^t - x_i^t), i = 2{:}N \end{cases} \quad (18)$$

where, ω_2 stands for a weighting factor for the cyclone related foraging. The representation of random position within the searching spaces can be expressed as following (Zhao et al., 2020):

$$x_{rand} = L_b + r.(U_b - L_b) \quad (19)$$

$$x_i^{t+1} = \begin{cases} x_{rand} + r.(x_{rand}^t - x_i^t) + \omega_2.(x_{rand}^t - x_i^t), i = 1 \\ x_{rand} + r.(x_{i-1}^t - x_i^t) + \omega_2.(x_{rand}^t - x_i^t), i = 2{:}N \end{cases}$$

where, U_b and L_b denote the upper and lower bounds for the searching space, respectively for the desired controllable variables, x_{rand} stands for the assigned randomly selected position within the searching space.

Thirdly, the somersault-related process of foraging can be determined as follows (Aly and Rezk, 2021):

$$x_i^{t+1} = x_i^t + S.(r_2 . x_{ibest}^t - r_3 . x_i^t), i = 1,2, \ldots\ldots, N \quad (20)$$

where, S denotes the somersault factor that is employed for the determination process of somersault ranges for the manta rays, whereas the variables r_2 and r_3 stand for randomly selected numbers.

2.3. 2. The Design of LFC Methods Using MRFO Algorithm

In this work, the MRFO algorithm is employed for the design process of the studied controllers. Figure 6 shows the complete optimization process of studied LFC methods. Whereas the entire MRFO algorithm is shown in Figure 7. The MRFO searches within the defined parameter limits for the optimum parameter combinations of the controller and hence optimizes the performance of overall power system frequency regulations. Firstly, the range of the search of each individual parameter is set and defined for the MRFO algorithm to search the optimum values within these ranges of each parameter. Secondly, the main driving objective function is adjusted and designed to control the criteria of the searching and convergence process of the MRFO algorithm. As the studied system consists of a single power area power grid system, the objective function includes the frequency deviation Δf of the studied area in its formulation. Therefore, a measure from the frequency deviation signal is feedback to the optimization process to define the best optimal solution within the maximum iteration number of the MRFO algorithm. Therefore, there is a single objective in the function for the driving process of the optimization algorithm during the simulation total time t_s while the problem constraints are considered during the optimization process. The defined objective function in this work is based on the integral-squared error function (ISE) as the driving objective of the algorithm as follows:

$$ISE = \text{integral squared error} = \int_0^{t_s} (\Delta {f_a}^2)\, dt \quad (21)$$

The representation diagram of the proposed design and parameter optimization processes based on using the MRFO algorithm is shown in Figure 5. The main constraints that are considered within the proposed design and parameters optimization processes are as follows:

$$\begin{aligned} {K_P}^{min} \le\ & K_P \le {K_P}^{max} \\ {K_I}^{min} \le\ & K_I \le {K_I}^{max} \\ {K_D}^{min} \le\ & K_D \le {K_D}^{max} \end{aligned} \quad (22)$$

where the lower/upper bounds of each tunable control parameter are expressed through the use of *min* and max symbols, respectively, for the designed LFC methods. The employed bounds for the minimum parameter values in the proposed method are set for ${K_P}^{min}$, ${K_I}^{min}$, and ${K_D}^{min}$ at zero value, and the maximum values are set for ${K_P}^{max}$, ${K_I}^{max}$, and ${K_D}^{max}$ at values of 5 during the proposed optimization and parameter determination process. Figure 8 shows the schematic diagram representation of the optimization process.

The various obtained LFC method parameters for the studied system and controllers are summarized in Table II, based on the use of the MRFO algorithm for each studied case.

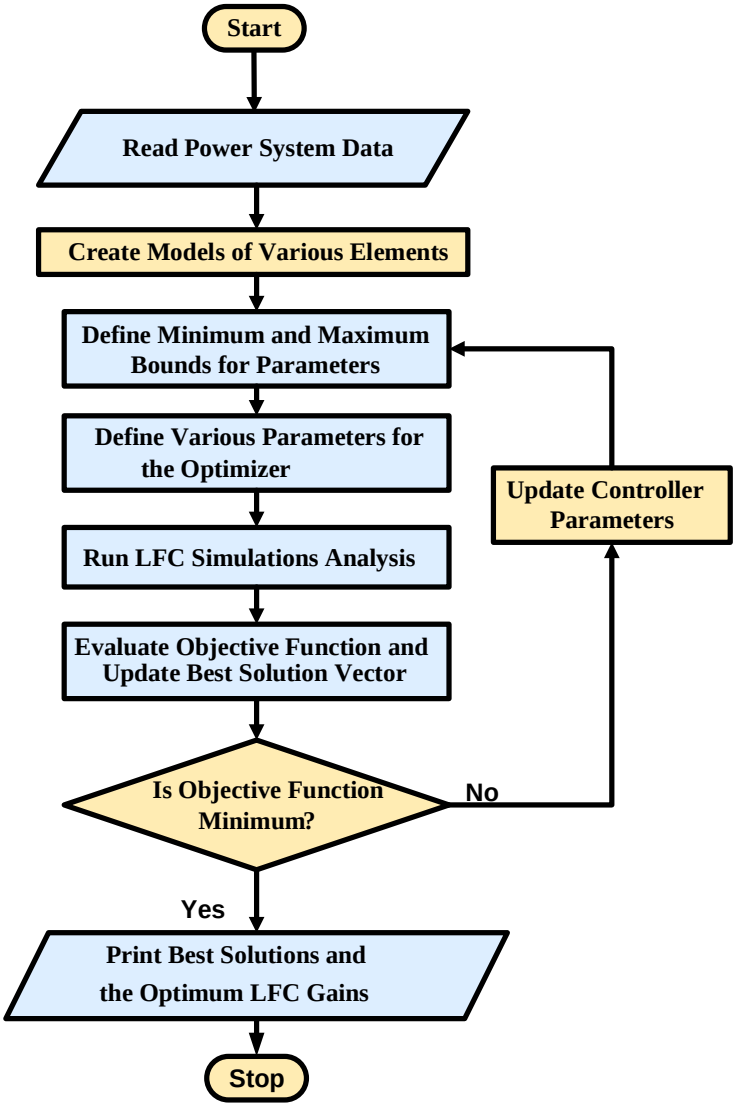

Fig. 6. The main steps of the parameters' optimization process.

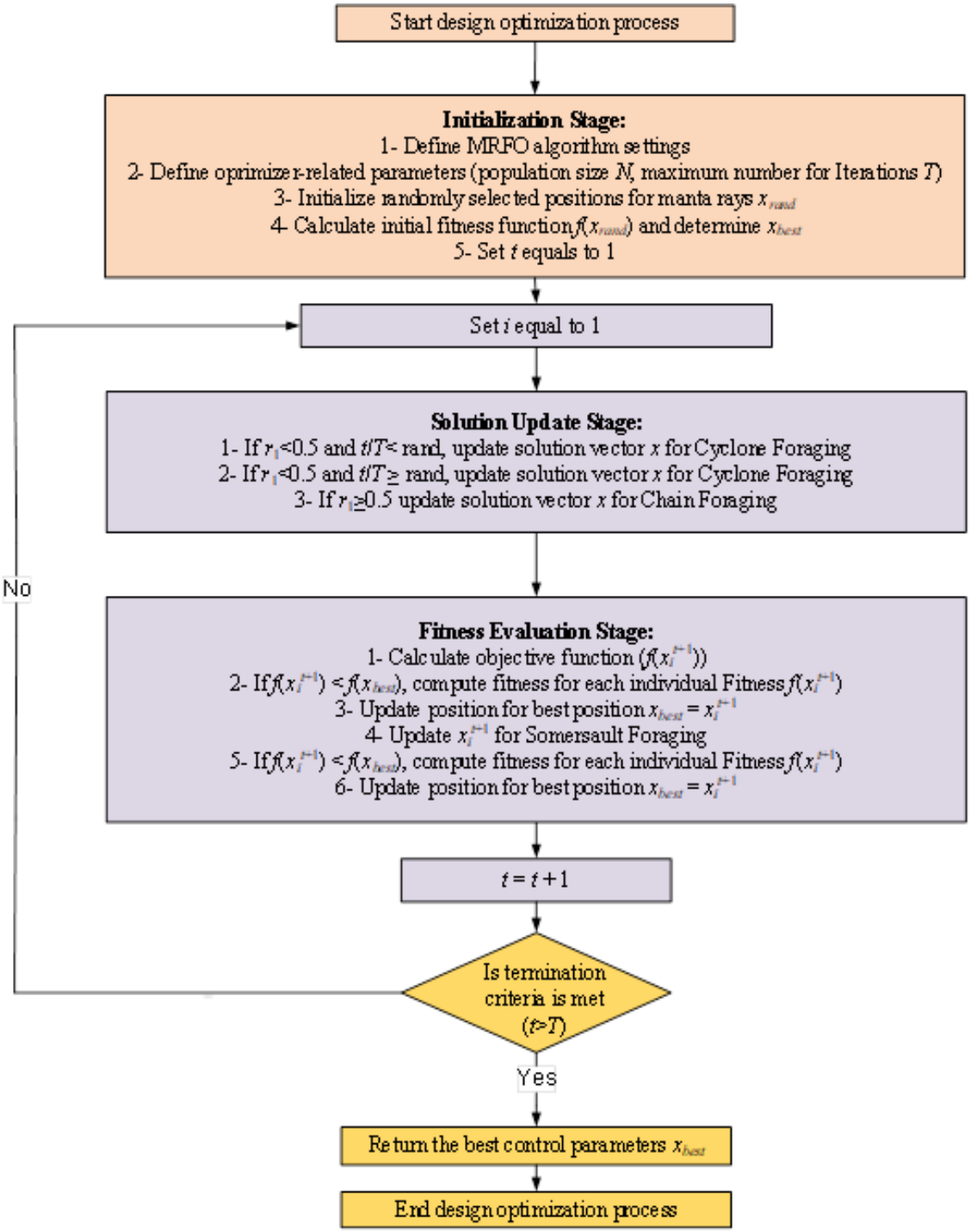

Fig. 7. The inherent operation of MRFO algorithm for parameters optimization process.

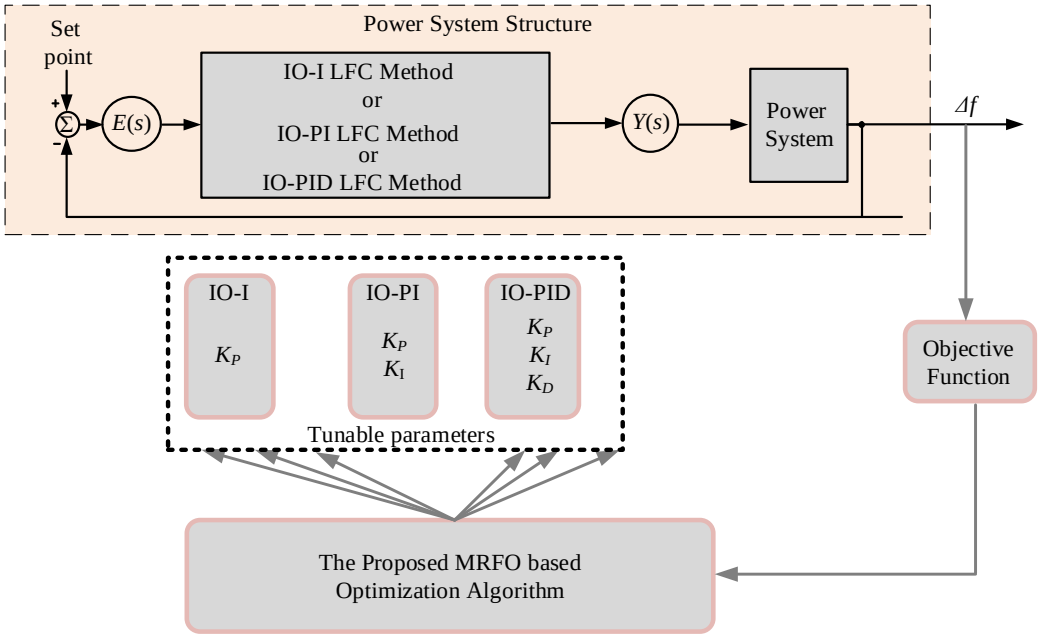

Fig. 8. The schematic diagram representation of the optimization process.

Table II. Obtained control parameters based on the MRFO algorithm

Controller	Parameter	Value
P IO-LFC	K_P	0.62
PI IO-LFC	K_P	4.312
	K_I	1.628
PID IO-LFC	K_P	4.862
	K_I	1.985
	K_D	0.531

2. 4. Communication Delay Modelling

The communication time delay, usually called latency, represents the amount of time taken by packets of data during their travel from one particular device to another over the network. Several factors, including the distance between devices, processing time, and network congestion cause the time delays. The main components in the definition of time delays include the following:

1. ***Transmission time delay***: It represents the time taken by packets of data during their transmission from one particular device to another device. It is defined by the required time for encoding and decoding data and the time taken for transmitting data over networks.
2. ***Propagation time delay***: It is defined by the time taken by signals to travel from a particular point in the network to another point. This is because light speed defines the limits of maximum speed for travelling data through communication networks. Therefore, signals will often need to take time for their propagation.

3. ***Queuing time delay***: It represents the time data packets wait in queues before their transmissions. Queuing delays happen when more packets exist than the network can handle. Therefore, packets need to await their transmissions.
4. ***Jitter time delay***: It represents the time delay by jitters resulting from networks congestions or by differences between the processing speeds among the communication devices. Some variations in the time delays exist between packets in communication system.

In this work, the communication delay is considered, and its effects on the LFC stability will be studied. Figure 9 shows the structure of the studied power system after adding the different communication channels. There is a channel in the sensed frequency signal to be sent for the load frequency controller through the communication channel. Another communication channel is considered for the output control signals to the various controllable generation units of the system.

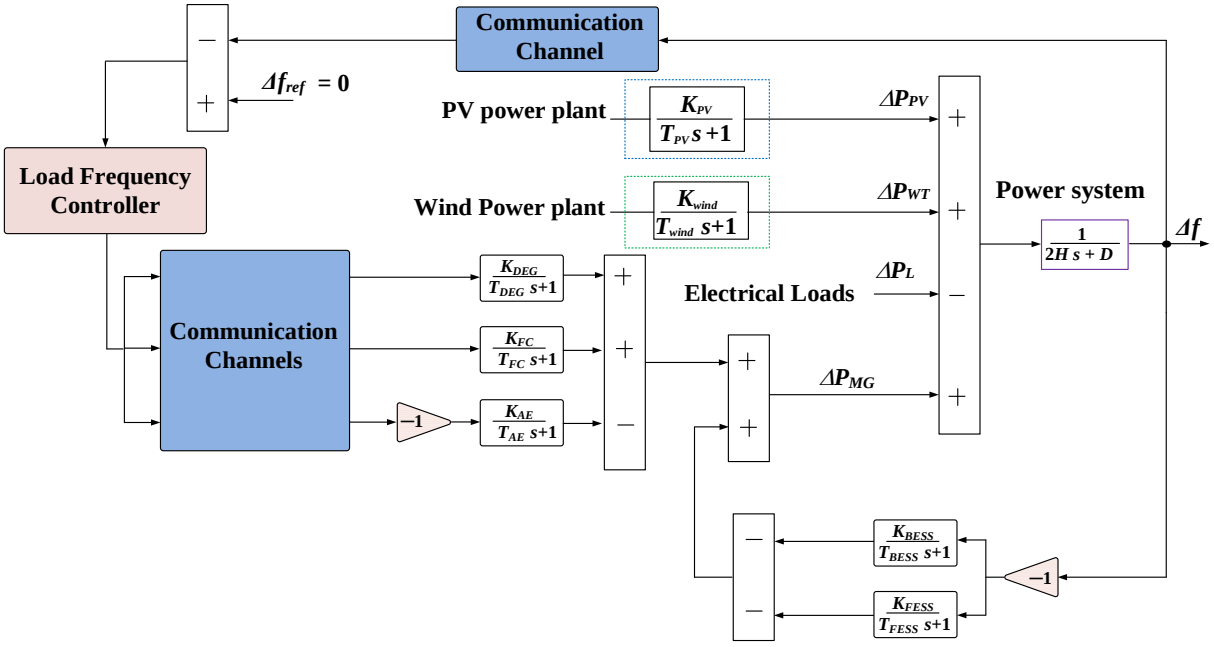

Fig. 9. The system structure with adding the communication channels and their related delays.

3. Results and Discussion

The obtained results are organized into 12 different scenarios to cover all the expected differences of disturbances. The system parameters in Table. I and the control parameters in Table II are employed in the results and proposed study. The main considered generation, loading, and system parameters scenarios are summarized as follows:

- **Scenario No. 1:** using 3 different types for controllers I, PI, and PID without delay at step load power (SLP).
- **Scenario No. 2:** using 3 different types for controllers I, PI, and PID with 1 delay, 1 delay (0.5 s) at SLP.
- **Scenario No. 3:** using 3 different types for controllers I, PI, and PID with two delays, 1 delay and 2 delays, (0.5 s) at SLP.

- **Scenario No. 4:** using 3 different types for controllers I, PI, and PID with different delay values without delay, 1 delay (0.1 s), 1 delay (0.5 s), 1 delay (1 s) at SLP.
- **Scenario No. 5:** using 3 different types for controllers I, PI, and PID without delay at PV variations.
- **Scenario No. 6:** using 3 different types for controllers I, PI, and PID with one delay, 1 delay (0.5 s) at PV variations.
- **Scenario No. 7:** using 3 different types for controllers I, PI, and PID with two delays, 1 delay and 2 delays, (0.5 s) at PV variations.
- **Scenario No. 8:** Using PID controller with different delay values without delay, 1 delay (0.1 s), 1 delay (0.5 s), 1 delay (1 s) at PV variations.
- **Scenario No. 9:** Using 3 different types for controllers I, PI, and PID without delay at wind variations.
- **Scenario No. 10:** Using 3 different types for controllers I, PI, and PID with one delay, 1 delay (0.5 s) at wind variations.
- **Scenario No. 11:** Using 3 different types for controllers I, PI, and PID with two delays, 1 delay and 2 delays, (0.5 s) at wind variations.
- **Scenario No. 12:** Using PID controller with different delay values without delay, 1 delay (0.1 s), 1 delay (0.5 s), 1 delay (1 s) at wind variations.

3. 1. Scenario No. 1: Using 3 different types for controllers I, PI, and PID without delay.

In this scenario, the studied microgrid system stability is examined via the change of step load perturbation (SLP) of 1% without the effect of any communication delay. Figure 10 shows the system frequency deviations utilizing different control techniques such as I, PI, and PID controllers. It can be monitored that the I controller suffers from the high-frequency deviations of +0.074 Hz and -0.12 Hz overshoot and undershoot, respectively, and cannot settle down to the normal value during the whole simulation time. While the PI controller has frequency variations less than the I controller, with around +0.04 Hz and -0.07 Hz, it can return the frequency to its normal value at 142 sec. The PID controller has the best effect as it can dampen the frequency oscillations to +0.022 Hz and -0.051 Hz and settle down at 81 sec. Table. III summarized the numerical data of this scenario for all control types without the effect of delay.

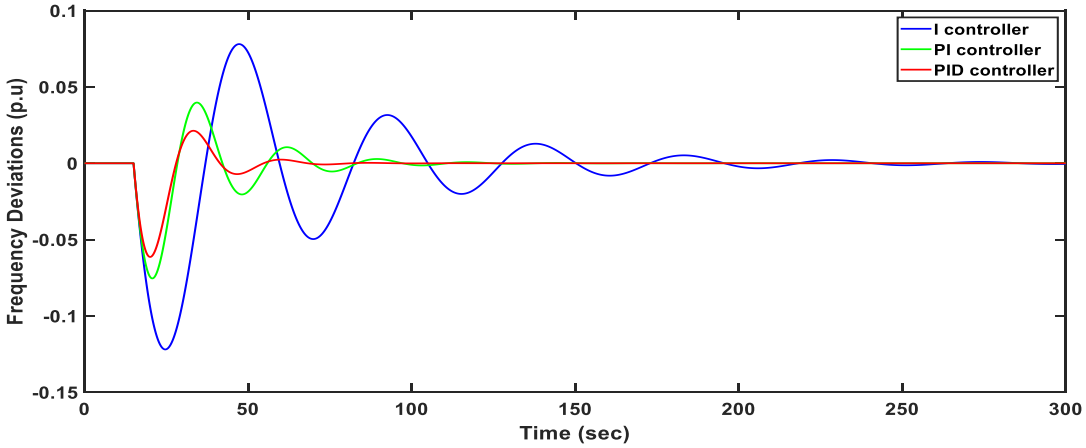

Fig. 10. Obtained results in scenario No. 1.

3. 2. Scenario No. 2: Using 3 different types for controllers I, PI, and PID with 1 delay (0.5 s)

This scenario studies the influence of a one-time delay signal on the performance of the suggested control structures at the studied microgrid system at an SLP of 1% change. This delay is connected through the feedback signal from the frequency change output. Hence, this scenario represents a challenging case for the controllers. Figure 11 depicts the dynamic response of the microgrid system. It can be detected from this figure that the PID controller has a positive impact on the frequency deviations despite the effect of time delay. However, the PI controller has a deviation of +0.05 Hz and 0.83 Hz with a long settling time. Furthermore, the I controller has a negative effect due to the presence of the time delay signal as the deviations increased to around +0.94 Hz and -0.13 Hz without returning to the nominal value of system frequency. This scenario shows the clear impact of the first-order delay signal on the dynamic performance of the examined microgrid system.

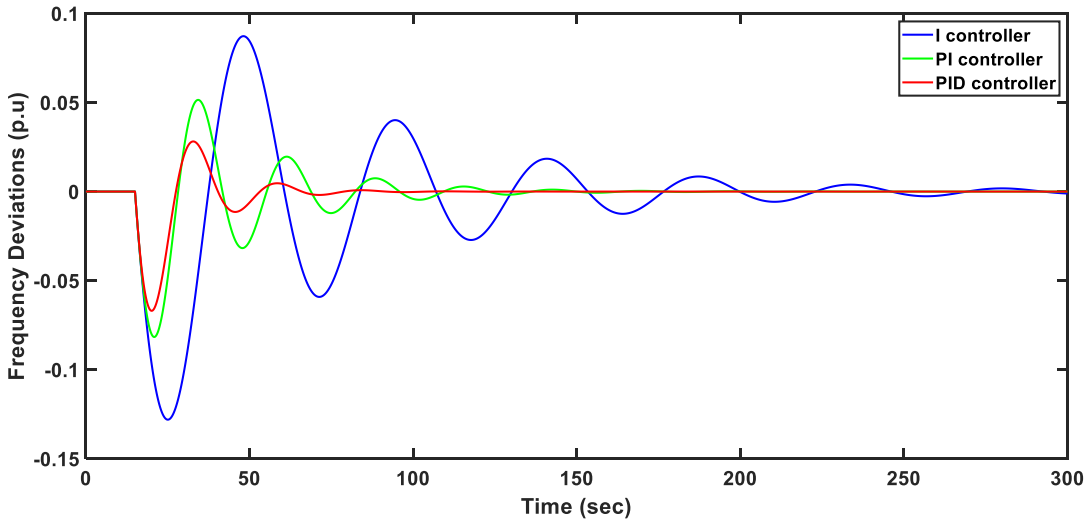

Fig. 11. Obtained results in scenario No. 2.

3. 3. Scenario No. 3: Using 3 different types for controllers I, PI, and PID with delay, 1 delay and 2 delays, (0.5 s)

This scenario studies the effect of two-time delay signals on the system performance; one of them is taken from the frequency deviation feedback signal, and the other is taken from the area control error signal with the same SLP of the previous scenarios. Figure 12 shows the impact of the two-time delay signals on the system frequency deviation utilizing the I, PI, and PID control methods. It can be noted that the influence of the double delay made the I controller suffer from more frequency oscillations in this case, with +0.099 Hz and -0.144 Hz, which are more than the previous two scenarios. Furthermore, the two-time delays have affected the PI type as it has many frequency fluctuations with an overshoot of 0.065 Hz, an undershoot of 0.09 Hz, and a very long settling time. On the other side, although the PID controller has higher oscillations than its performance in the previous two scenarios, it still has the best performance among the other controllers in the two scenarios of time delay signals, as summarized in Table. III for numerical data of this case.

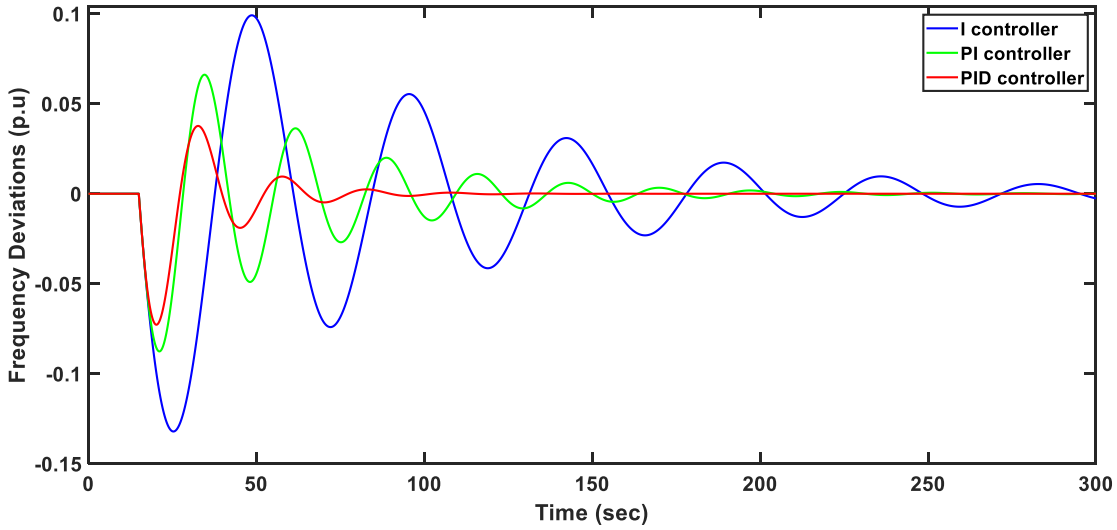

Fig. 12. Obtained results in scenario No. 3.

Table III. System results for scenarios 1, 2, and 3 of SLP

Controller	**I**			**PI**			**PID**		
Data	Without delay	1 delay	2 delays	Without delay	1 delay	2 delays	Without delay	1 delay	2 delays
Overshot (p.u.)	0.07	0.09	0.1	0.04	0.05	0.07	0.02	0.035	0.045
Settling time (s)	250	300	350	125	155	280	70	100	135
Ripples start to stable (s)	3	5	8	3	5	8	3	4	6

3. 4. Scenario No. 4: Using 3 different types for controllers I, PI, and PID with different delay values

In this scenario, the change in time delay value and its impact on the interpretation of the three suggested controllers have been analyzed. Figure 13(a) shows the time delay effect on the I controller at values (0.1 s, 0.5 s, 1 s, and without delay). It can be seen that the increasing time delay causes an increase in overshot and undershoot values of frequency deviations and takes a very long time to settle down. The PI controller has a negative effect on the change values of communication time delay, especially at the delay of one, which makes the system frequency deviations go to infinity, as depicted in Figure 13(b). Furthermore, as shown in Figure 13(c), the PID controller is affected by different time delay values. However, it still has the best performance compared to the I and PI control methods. It is evident that the microgrid system frequency deviations are quickly brought back to their initial value after less time, which shows that the optimized PID controller guarantees the studied microgrid stability.

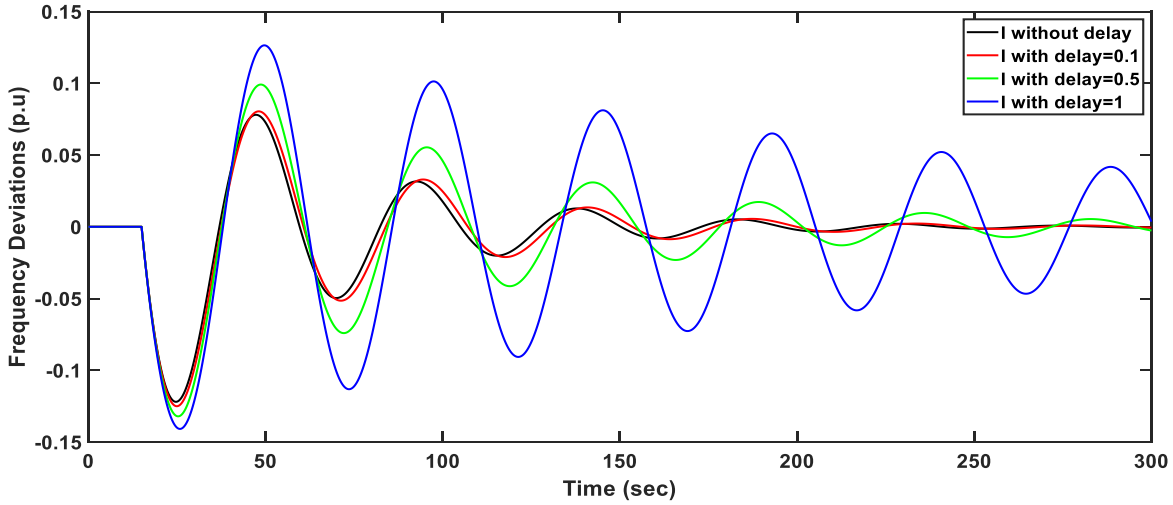

(a). I controller

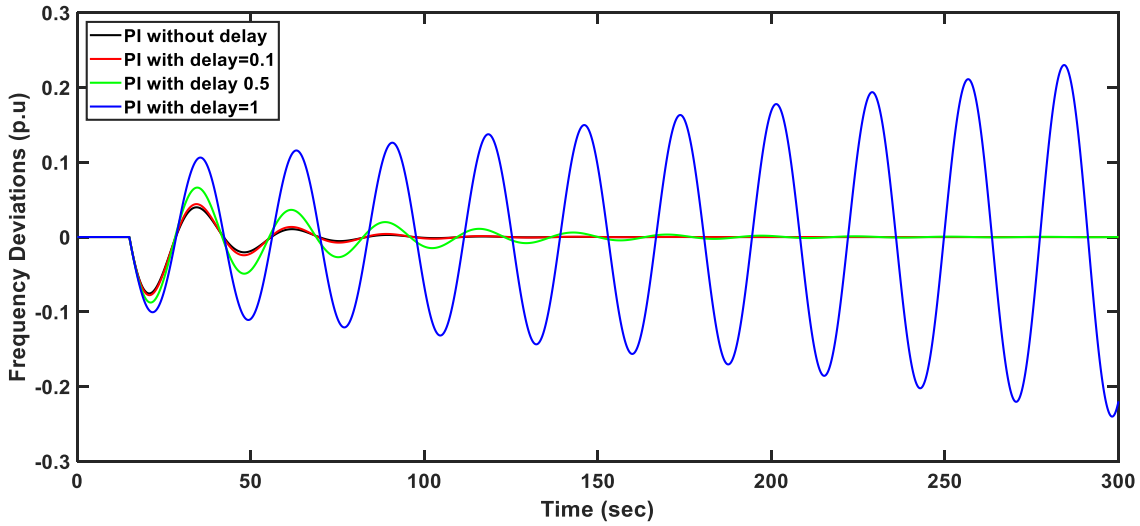

(b). PI controller

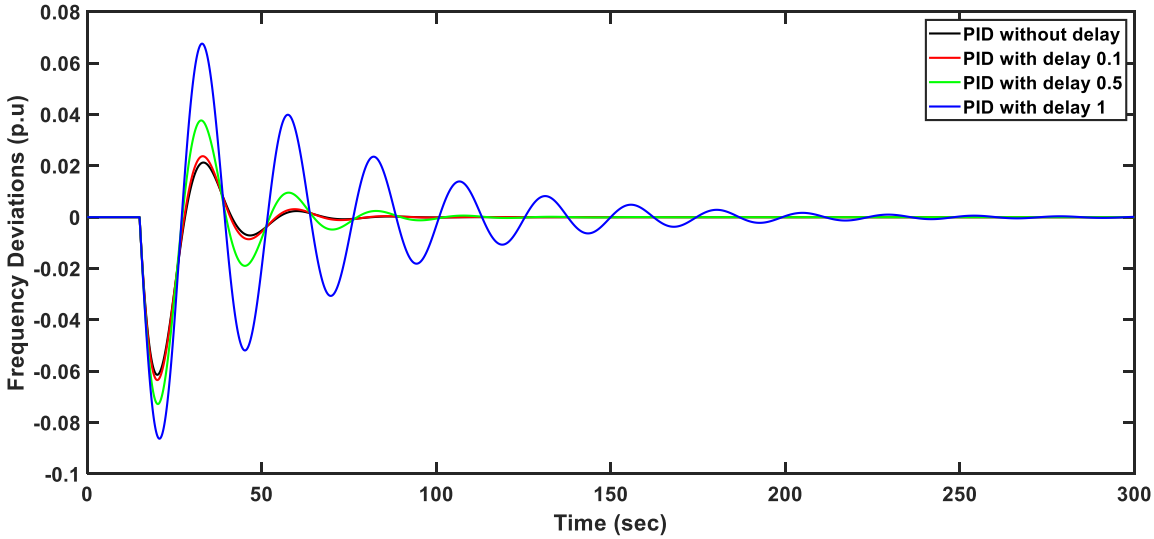

(c). PID controller

Fig. 13. Obtained results at scenario No. 4.

3. 5. Scenario No. 5: Using 3 different types for controllers I, PI, and PID without delay using PV generation

Figure 14 shows the system frequency deviations without the effect of delay using the three controllers. I, PI, and PID controllers take into consideration the fluctuations of the RESs generation. The PV unit with 0.02 p.u is connected at a time of 20 s, as shown in Figure 14(a). From Figure 14(b), it can be observed from this figure that the PID controller has the best performance as it can diminish the frequency peak to lower values than the I and PI controllers with less settling time.

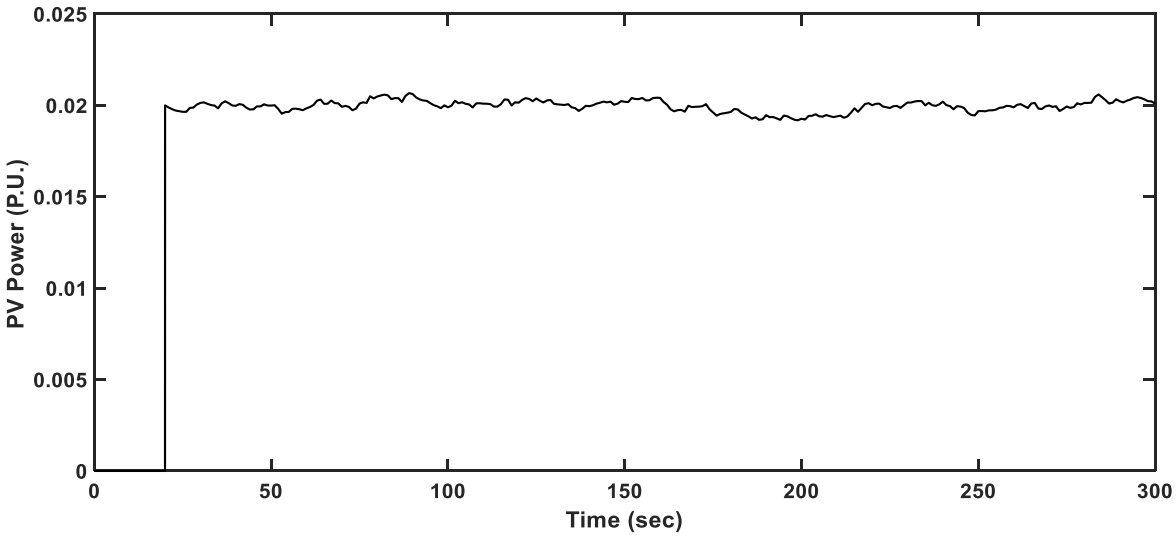

(a). PV power

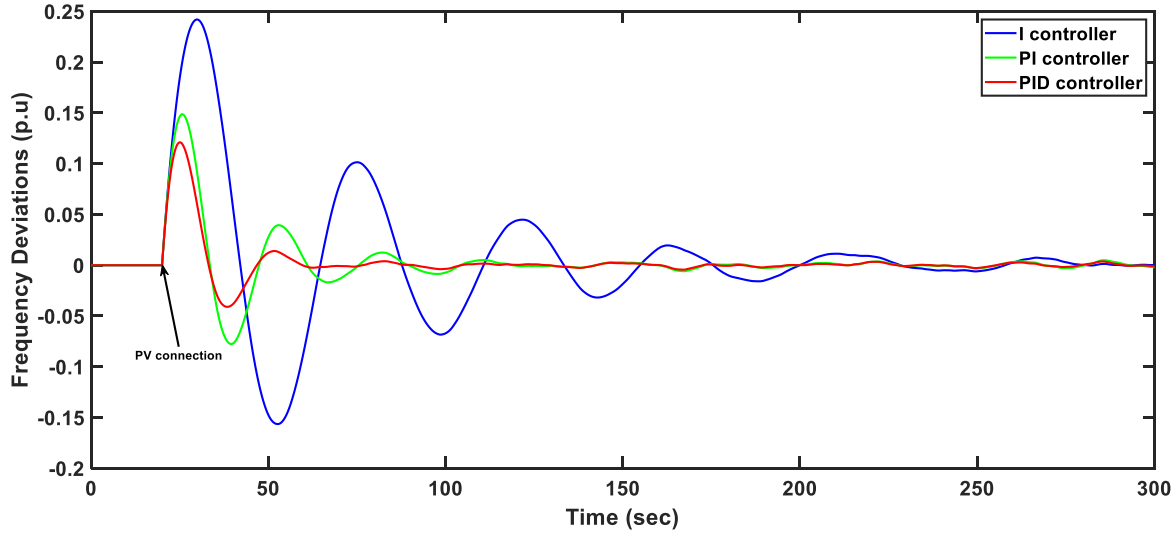

(b). System response

Fig. 14. Obtained results at scenario No. 5.

3. 6. Scenario No. 6: Using 3 different types for controllers I, PI, and PID with 1 delay (0.5 s) with PV fluctuations

This case shows the effect of using one communication time delay with the fluctuated PV power on the performance of the three controllers. The time delay is 0.5 s with connecting PV unit at 20 secs of simulation time. It can be noted that using a time delay made the frequency have more

deviations with a long settling time to its normal value. On the other side, the PID controller still has the best performance in damping the large PV oscillations despite the effect of delay signal as depicted in Figure 14 and Table. IV.

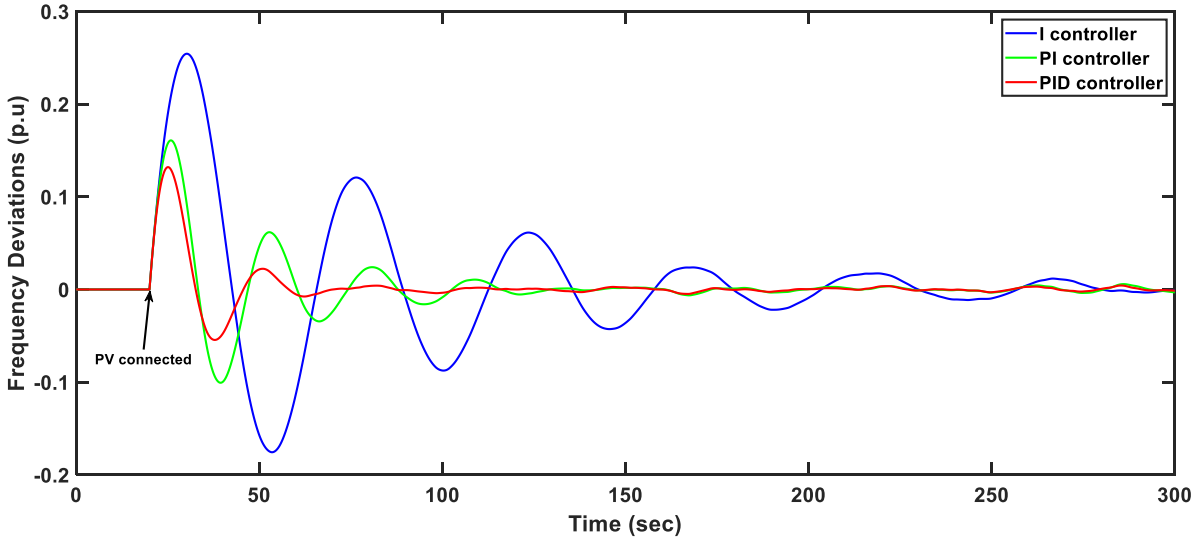

Fig. 15. Obtained results at scenario No. 6.

3. 7. Scenario No. 7: Using 3 different types for controllers I, PI, and PID with delay, 1 delay and 2 delays, (0.5 s) with PV fluctuations

This case examines the effect of two-time delay signals on the system performance; one of them is taken from the 'f feedback signal, and the other is taken from the *ACE* signal with the same PV oscillations of the previous scenarios 5 and 6. Figure 16 shows the effect of using two-time delay signals on the system frequency deviancy comparing I, PI, and PID controllers. It is obvious the influence of the double delay on the performance of the system and controllers. The I controller bears higher frequency oscillations via this scenario with +0.26 Hz and -0.199 Hz than scenarios 5 and 6. Furthermore, the PI type has been disturbed by the two-time delays as it has lots of frequency fluctuations with an overshoot of 0.173 Hz and undershoot of 0.13 Hz with a long stability time. Even if the PID controller has higher frequency vacillations than the performance in the earlier two scenarios, it is still gaining the best one among the other methods in the two scenarios of one- and two-time delay signals, as summarized in Table. IV for numerical data of this case.

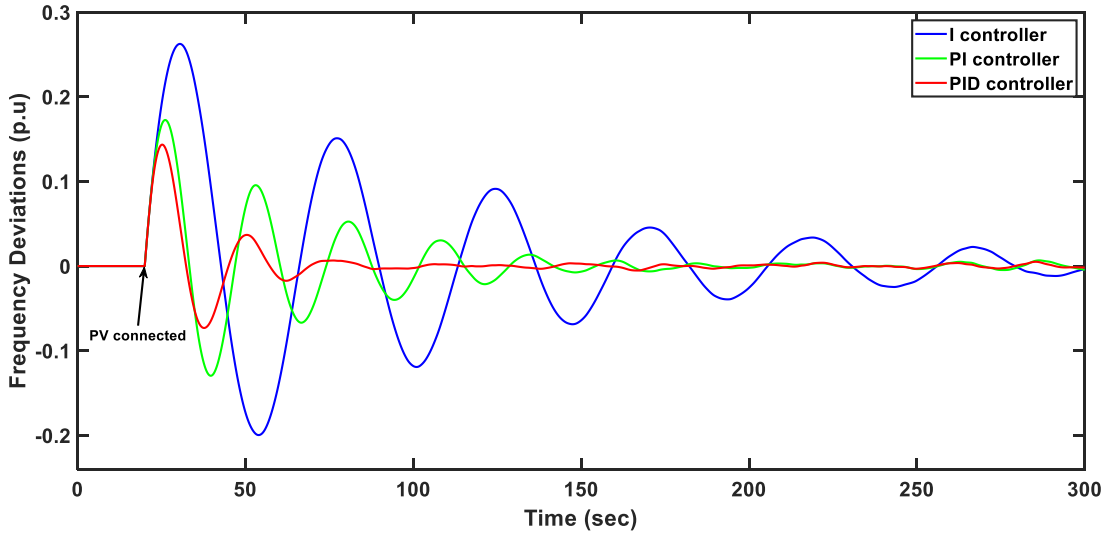

Fig. 16. Obtained results at scenario No. 7.

3. 8. Scenario No. 8: Using PID controller without delay, delay (0.1 s), delay (0.5 s), and delay (1 s), at PV fluctuation case

In this scenario, the communication time delay value is changed between (0.1 s, 0.5 s, 1 s, and without delay) to check its impact on the system performance and the action of each suggested controller on the frequency regulation. Figure 17 compares I, PI, and PID controllers with different values of the time delay signal. It can be seen that the increasing of time delay produces more disturbance in frequency in terms of overshoot, undershoot, and settling time values. Whereas I controller has an increase in frequency perversions and picks a very long time to settle down. While the PI controller comes second after the I type as it can damp the oscillations better and faster than the I controller. As shown in the figure, the PID controller is already affected by increasing the time delay. However, it can demoralize the frequency deviations quickly and with lower over/undershoots than the other methods.

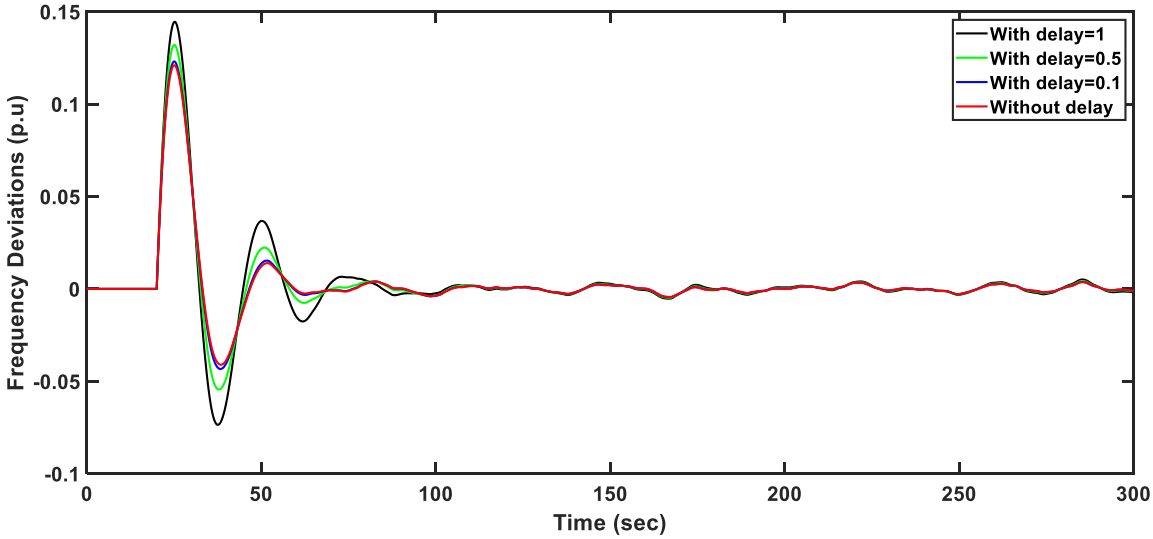

Fig. 17. Obtained results at scenario No. 8.

3. 9. Scenario No. 9: Using 3 different types for controllers I, PI, and PID without delay using wind generation

This case considers a severe situation of high wind speed fluctuations to validate the performance of the utilized controllers I, PI, and PID controllers with all cases of suggested communication time delay values. Therefore, the wind generator is connected to the system at the time of 50 s without utilizing the communication delay. Figure 18(a) shows the wind generation profile for this case. It is clear from Figure 18(b) that at the instant of inserting the wind power at 50 sec, the frequency deviates to high overshoot and undershoot values. The I controller has frequency overshoot for more than +0.23 Hz, PI with +0.16 Hz, and PID with +0.1 Hz beside undershoots of -0.18 Hz, -0.09 Hz, and -0.03 Hz, respectively.

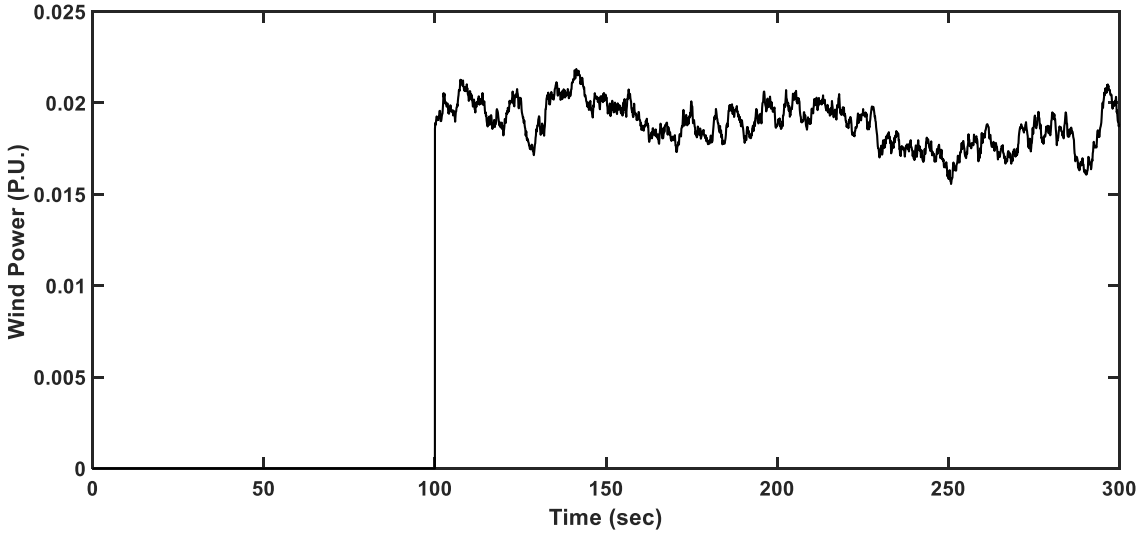

(a). Wind power

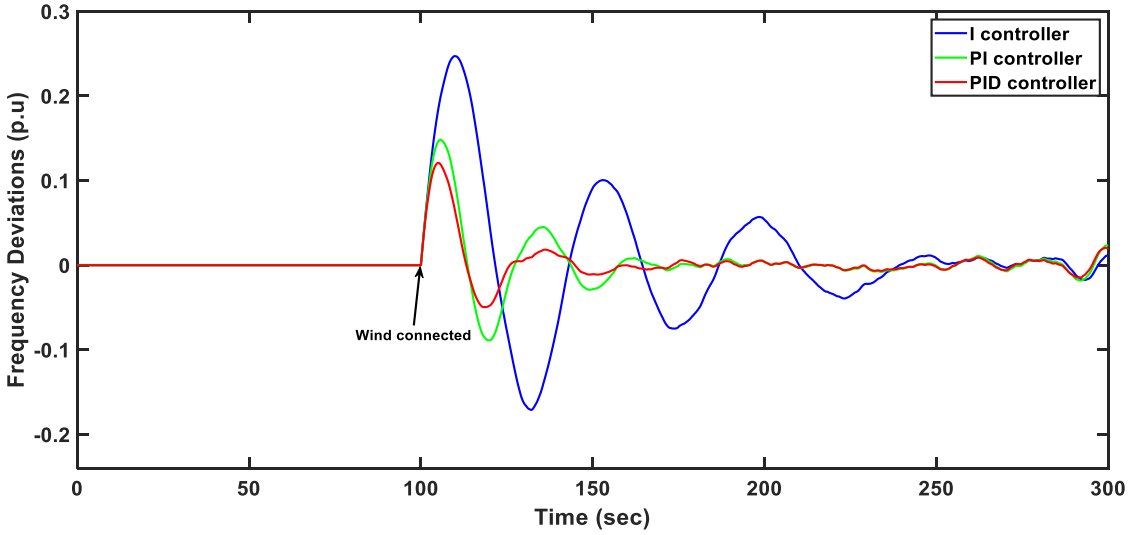

(b). System response

Fig. 18. Obtained results at scenario No. 9.

Table IV. System results for scenarios 5, 6, and 7 of PV fluctuations

Controller	**I**			**PI**			**PID**		
Data	Without delay	1 delay	2 delays	Without delay	1 delay	2 delays	Without delay	1 delay	2 delays
Overshot (p.u.)	0.24	0.27	0.285	0.15	0.17	0.182	0.12	0.125	0.132
Settling time (s)	310	345	370	145	175	255	130	165	195
Ripples start to stable (s)	3	5	8	3	5	8	3	4	6

3. 10. Scenario No. 10: Using 3 different types for controllers I, PI, and PID with delay of (0.5 s), using wind generation

This scenario discusses the utilizing of communication time delay of (T_{dd1} = 0.5 s) while applying the wind power at 50 s. The system frequency divergence increases to high values due to the using of time delay as depicted in Figure 19. This figure shows a performance comparison of I, PI, and PID control methods. It can be observed that the PID controller has significantly reduced the maximum overshoot, undershoot, and settling time of the system frequency. While the I and PID controllers have high frequency deviations with long settling times.

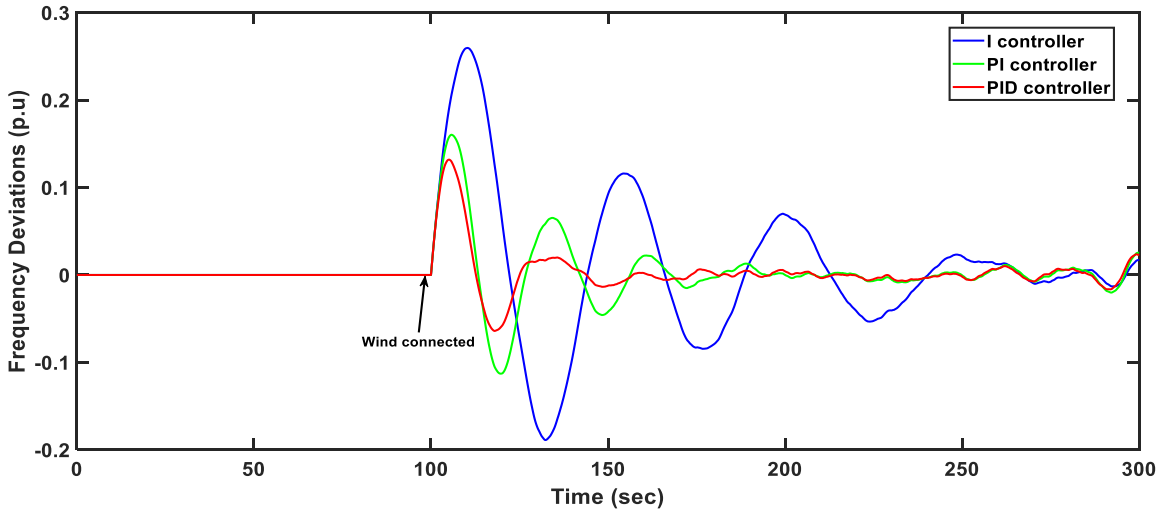

Fig. 19. Obtained results at scenario No. 10.

3. 11. Scenario No. 11: Using 3 different types for controllers I, PI, and PID with two delay times of (0.5 s), using wind generation

In this scenario, two delay time signals were applied to the high-fluctuated wind generation to validate the performance of all suggested controllers. Figure 20 shows the system frequency in this case. It can be noted that the system frequency changes return to normal with the least

oscillation and in the shortest settling time when utilizing the PID technique, while with other controllers, the frequency has more fluctuations and returns to normal later.

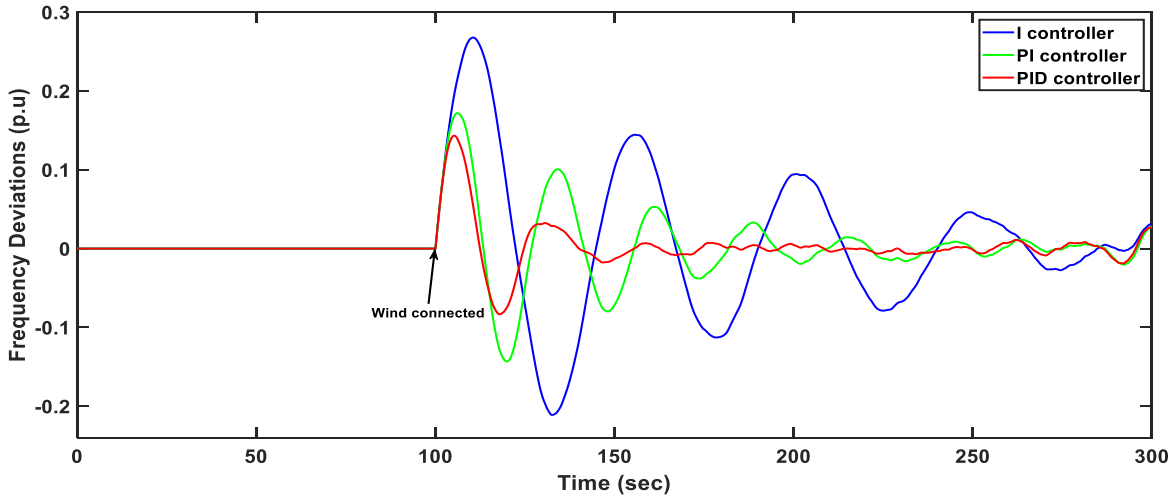

Fig. 20. Obtained results at scenario No. 11.

Table V. System results for scenarios 9, 10, and 11 of PV fluctuations

Controller	**I**			**PI**			**PID**		
Data	Without delay	1 delay	2 delays	Without delay	1 delay	2 delays	Without delay	1 delay	2 delays
Overshot (p.u.)	0.25	0.275	0.283	0.143	0.162	0.179	0.115	0.131	0.136
Settling time (s)	FU	FU	FU	240	270	298	215	235	255
Ripples start to stable (s)	3	5	8	3	5	8	3	4	6

3. 12. Scenario No. 12: Using PID controller without delay, delay (0.1 s), delay (0.5 s), and delay (1 s), at wind fluctuation case

This scenario examines the performance of the PID controller as it represents the best controller in the previous scenarios. Therefore, it tested under the impact of high wind speed fluctuations and the increasing time delay signal until one. Figure 21 shows that the increasing time delay increases the overshot and undershoot of the frequency deviations as well as the settling time. However, the PID controller returned the deviation of the system frequency to its normal values with less time and overshoot and undershoot values with fewer differences. The performance of the suggested controllers with and without the time delay limits is analyzed via this study, which indicates the deterioration of the system's dynamic performance. Therefore, communication delays must be included in a realistic study of power microgrid systems.

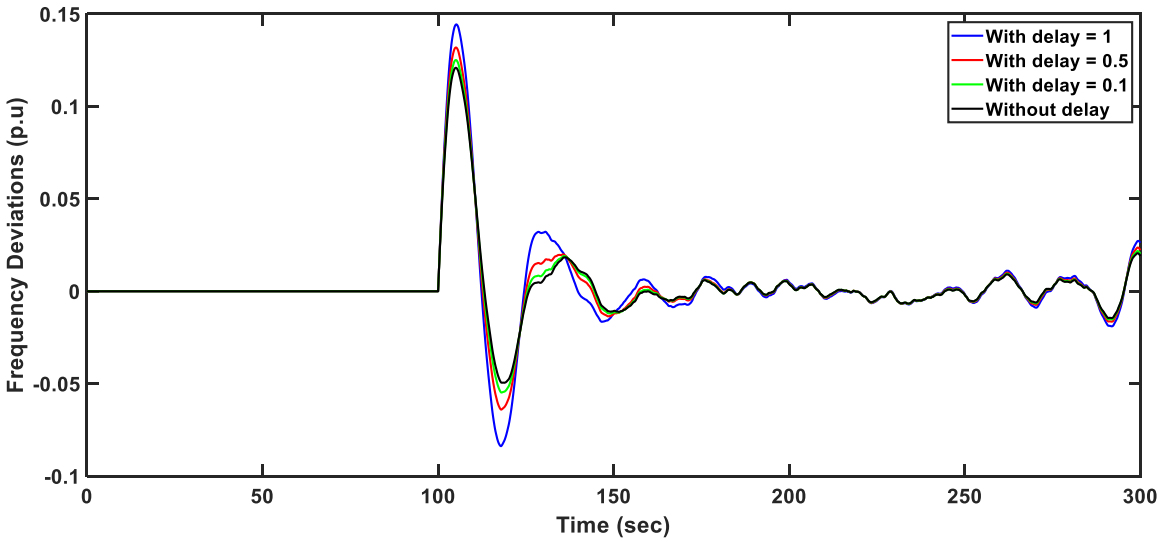

Fig. 21. Obtained results at scenario No. 12.

4. Conclusion

In this paper, the manta ray foraging optimizer algorithm (MRFO) is proposed for designing optimized load frequency controllers (LFC) in high renewable energy sources (RES) penetration levels power grids. Three widely presented LFC methods, namely the integral (I), proportional-integral (PI), and proportional-integral-derivative (PID) LFC methods, have been designed, evaluated, and compared in different possible operation scenarios. The effects of different communication channel delays are studied at different delay values, locations, and possibilities for the three studied LFC methods. The results showed that the consideration of communication delays determines, to a wide extent, the system stability and design sensitivity. In addition, the continuous variations in RES power are considered in this paper in addition to the existing energy storage systems employed for regulating the power system frequency. Different possible load power, generation power, values, and locations of communication delays are considered and compared in the paper. The overshot, rising time and time to stabilization are measured for all the studied scenarios. For instance, the PID controller has an overshot of 0.23 without considering a single communication delay and 0.132 with its consideration of fluctuated PV power. Whereas the I and PI controllers have higher overshot values of 0.24 and 0.15, respectively without communication delays in the same scenario. Considering communication delays showed higher overshot and rising time compared to ignoring its effects. Future results include extending the study for fractional order controllers and other advanced control methods. In addition, developing new hybrid control methods can be studied in future research with improved and detailed communication delay models.

References:

Abid, S., El-Rifaie, A.M., Elshahed, M., Ginidi, A.R., Shaheen, A.M., Moustafa, G., Tolba, M.A. (2023). Development of Slime Mold Optimizer with Application for Tuning Cascaded PD-PI Controller to Enhance Frequency Stability in Power Systems. Mathematics 11, 1796. https://doi.org/10.3390/math11081796

Advanced Frequency Regulation Strategies in Renewable-Dominated Power Systems (2024). Elsevier. https://doi.org/10.1016/C2021-0-02707-3

Ahmed, E.M., Mohamed, E.A., Selim, A., Aly, M., Alsadi, A., Alhosaini, W., Alnuman, H., Ramadan, H.A. (2023). Improving load frequency control performance in interconnected power systems with a new optimal high degree of freedom cascaded FOTPID-TIDF controller. Ain Shams Eng. J. 14, 102207. https://doi.org/10.1016/j.asej.2023.102207

Ahmed, E.M., Selim, A., Alnuman, H., Alhosaini, W., Aly, M., Mohamed, E.A., (2022). Modified Frequency Regulator Based on TIλ-TDμFF Controller for Interconnected Microgrids with Incorporating Hybrid Renewable Energy Sources. Mathematics 11, 28. https://doi.org/10.3390/math11010028

Almasoudi, F.M., Bakeer, A., Magdy, G., Alatawi, K.S.S., Shabib, G., Lakhouit, A., Alomrani, S.E., (2024). Nonlinear coordination strategy between renewable energy sources and fuel cells for frequency regulation of hybrid power systems. Ain Shams Eng. J. 15, 102399. https://doi.org/10.1016/j.asej.2023.102399

Almasoudi, F.M., Magdy, G., Bakeer, A., Alatawi, K.S.S., Rihan, M., (2023). A New Load Frequency Control Technique for Hybrid Maritime Microgrids: Sophisticated Structure of Fractional-Order PIDA Controller. Fractal Fract. 7, 435. https://doi.org/10.3390/fractalfract7060435

Aly, M., Mohamed, E.A., Noman, A.M., Ahmed, E.M., El-Sousy, F.F.M., Watanabe, M., (2023a). Optimized Non-Integer Load Frequency Control Scheme for Interconnected Microgrids in Remote Areas with High Renewable Energy and Electric Vehicle Penetrations. Mathematics 11, 2080. https://doi.org/10.3390/math11092080

Aly, M., Mohamed, E.A., Noman, A.M., Ahmed, E.M., El-Sousy, F.F.M., Watanabe, M., (2023b). Optimized Non-Integer Load Frequency Control Scheme for Interconnected Microgrids in Remote Areas with High Renewable Energy and Electric Vehicle Penetrations. Mathematics 11, 2080. https://doi.org/10.3390/math11092080

Aly, M., Rezk, H., (2021). A MPPT based on optimized FLC using manta ray foraging optimization algorithm for thermo-electric generation systems. Int. J. Energy Res. er.6728. https://doi.org/10.1002/er.6728

Aly, M., Rezk, H., (2020). A Differential Evolution-Based Optimized Fuzzy Logic MPPT Method for Enhancing the Maximum Power Extraction of Proton Exchange Membrane Fuel Cells. IEEE Access 8, 172219–172232. https://doi.org/10.1109/ACCESS.2020.3025222

Arora, K., Kumar, A., Kamboj, V.K., Prashar, D., Shrestha, B., Joshi, G.P., (2021). Impact of Renewable Energy Sources into Multi Area Multi-Source Load Frequency Control of Interrelated Power System. Mathematics 9, 186. https://doi.org/10.3390/math9020186

Arya, Y., Singh, K., (2024). A new SSA-based CFFOPID drop deloaded tidal turbine controller using HVDC-link. ISA Trans. S0019057824003367. https://doi.org/10.1016/j.isatra.2024.07.015

Bakeer, A., Magdy, G., Chub, A., Jurado, F., Rihan, M., (2022). Optimal Ultra-Local Model Control Integrated with Load Frequency Control of Renewable Energy Sources Based Microgrids. Energies 15, 9177. https://doi.org/10.3390/en15239177

Bakeer, M., Bakeer, A., Magdy, G., Aly, M.M., (2023). A new cyber-security approach for load frequency control of hybrid interconnected renewable power systems. J. Clean. Prod. 425, 138866. https://doi.org/10.1016/j.jclepro.2023.138866

Choudhary, R., Rai, J.N., Arya, Y., (2023). FOPTID+1 controller with capacitive energy storage for AGC performance enrichment of multi-source electric power systems. Electr. Power Syst. Res. 221, 109450. https://doi.org/10.1016/j.epsr.2023.109450

Choudhary, R., Rai, J.N., Arya, Y., (2022). Cascade FOPI-FOPTID controller with energy storage devices for AGC performance advancement of electric power systems. Sustain. Energy Technol. Assess. 53, 102671. https://doi.org/10.1016/j.seta.2022.102671

Ebeed, M., Hashem, M., Aly, M., Kamel, S., Jurado, F., Mohamed, E.A., Abd El Hamid, A.M., (2024). Optimal integrating inverter-based PVs with inherent DSTATCOM functionality for reliability and security improvement at seasonal uncertainty. Sol. Energy 267, 112200. https://doi.org/10.1016/j.solener.2023.112200

El Yakine Kouba, N., Menaa, M., Hasni, M., Boudour, M., (2015). Optimal load frequency control based on artificial bee colony optimization applied to single, two and multi-area interconnected power systems, in: 2015 3rd International Conference on Control, Engineering & Information Technology (CEIT). Presented at the 2015 3rd International Conference on Control, Engineering & Information Technology (CEIT), IEEE, Tlemcen, pp. 1–6. https://doi.org/10.1109/CEIT.2015.7233027

El-Sousy, F.F.M., Alqahtani, M.H., Aljumah, A.S., Aly, M., Almutairi, S.Z., Mohamed, E.A., (2023a). Design Optimization of Improved Fractional-Order Cascaded Frequency Controllers for Electric Vehicles and Electrical Power Grids Utilizing Renewable Energy Sources. Fractal Fract. 7, 603. https://doi.org/10.3390/fractalfract7080603

El-Sousy, F.F.M., Aly, M., Alqahtani, M.H., Aljumah, A.S., Almutairi, S.Z., Mohamed, E.A., (2023b). New Cascaded 1+PII2D/FOPID Load Frequency Controller for Modern Power Grids including Superconducting Magnetic Energy Storage and Renewable Energy. Fractal Fract. 7, 672. https://doi.org/10.3390/fractalfract7090672

Hassan, A., Aly, M.M., Alharbi, M.A., Selim, A., Alamri, B., Aly, M., Elmelegi, A., Khamies, M., Mohamed, E.A., (2023). Optimized Multiloop Fractional-Order Controller for Regulating Frequency in Diverse-Sourced Vehicle-to-Grid Power Systems. Fractal Fract. 7, 864. https://doi.org/10.3390/fractalfract7120864

Mohamed, E.A., Shawky, A., Almutairi, S.Z., Aly, M., Ahmed, E.M., Kandil, T., Hassan, M.S., (2023a). Optimal 1+PDDF/FOPIT frequency regulator for developing robust multi-microgrid systems with employing EV energy storage batteries. J. Energy Storage 73, 109088. https://doi.org/10.1016/j.est.2023.109088

Mohamed, E.A., Shawky, A., Almutairi, S.Z., Aly, M., Ahmed, E.M., Kandil, T., Hassan, M.S., (2023b). Optimal 1+PDDF/FOPIT frequency regulator for developing robust multi-

microgrid systems with employing EV energy storage batteries. J. Energy Storage 73, 109088. https://doi.org/10.1016/j.est.2023.109088

Nasiri Avanaki, I., Sarvi, M., (2016). A New Maximum Power Point Tracking Method for PEM Fuel Cells Based On Water Cycle Algorithm. J. Renew. Energy Environ. 3. https://doi.org/10.30501/jree.2016.70076

Nasirov, S., Agostini, C., Silva, C., Caceres, G., (2018). Renewable energy transition: a market-driven solution for the energy and environmental concerns in Chile. Clean Technol. Environ. Policy 20, 3–12. https://doi.org/10.1007/s10098-017-1434-x

Nayak, S.R., Khadanga, R.K., Arya, Y., Panda, S., Sahu, P.R., (2023a). Influence of ultra-capacitor on AGC of five-area hybrid power system with multi-type generations utilizing sine cosine adopted dingo optimization algorithm. Electr. Power Syst. Res. 223, 109513. https://doi.org/10.1016/j.epsr.2023.109513

Nayak, S.R., Khadanga, R.K., Das, D., Arya, Y., Panda, S., Sahu, P.R., (2023b). Influence of Ultracapacitor and Plug-In Electric Vehicle for Frequency Regulation of Hybrid Power System Utilizing Artificial Gorilla Troops Optimizer Algorithm. Int. J. Energy Res. 2023, 1–18. https://doi.org/10.1155/2023/6689709

Noman, A.M., Aly, M., Alqahtani, M.H., Almutairi, S.Z., Aljumah, A.S., Ebeed, M., Mohamed, E.A., (2024). Optimum Fractional Tilt Based Cascaded Frequency Stabilization with MLC Algorithm for Multi-Microgrid Assimilating Electric Vehicles. Fractal Fract. 8, 132. https://doi.org/10.3390/fractalfract8030132

Nour, M., Magdy, G., Bakeer, A., Telba, A.A., Beroual, A., Khaled, U., Ali, H., (2023a). A New Fractional-Order Virtual Inertia Support Based on Battery Energy Storage for Enhancing Microgrid Frequency Stability. Fractal Fract. 7, 855. https://doi.org/10.3390/fractalfract7120855

Nour, M., Magdy, G., Chaves-Ávila, J.P., Sánchez-Miralles, Á., Jurado, F., (2023b). A new two-stage controller design for frequency regulation of low-inertia power system with virtual synchronous generator. J. Energy Storage 62, 106952. https://doi.org/10.1016/j.est.2023.106952

Pan, I., Das, S., (2016). Fractional Order AGC for Distributed Energy Resources Using Robust Optimization. IEEE Trans. Smart Grid 7, 2175–2186. https://doi.org/10.1109/TSG.2015.2459766

Rangi, S., Jain, S., Arya, Y., (2024). Utilization and performance comparison of several HESSs with cascade optimal-FOD controller for multi-area multi-source power system under deregulated environment. J. Energy Storage 94, 112469. https://doi.org/10.1016/j.est.2024.112469

Ray, P.K., Mohanty, S.R., Kishor, N., (2011). Proportional–integral controller based small-signal analysis of hybrid distributed generation systems. Energy Convers. Manag. 52, 1943–1954. https://doi.org/10.1016/j.enconman.2010.11.011

Sahoo, G., Sahu, R.K., Panda, S., Samal, N.R., Arya, Y., (2023). Modified Harris Hawks Optimization-Based Fractional-Order Fuzzy PID Controller for Frequency Regulation of

Multi-Micro-Grid. Arab. J. Sci. Eng. 48, 14381–14405. https://doi.org/10.1007/s13369-023-07613-2

Sahu, R.K., Panda, S., Rout, U.K., Sahoo, D.K., (2016). Teaching learning based optimization algorithm for automatic generation control of power system using 2-DOF PID controller. Int. J. Electr. Power Energy Syst. 77, 287–301. https://doi.org/10.1016/j.ijepes.2015.11.082

Salama, H.S., Magdy, G., Bakeer, A., Vokony, I., (2022). Adaptive coordination control strategy of renewable energy sources, hydrogen production unit, and fuel cell for frequency regulation of a hybrid distributed power system. Prot. Control Mod. Power Syst. 7, 34. https://doi.org/10.1186/s41601-022-00258-7

Shabani, H., Vahidi, B., Ebrahimpour, M., (2013). A robust PID controller based on imperialist competitive algorithm for load-frequency control of power systems. ISA Trans. 52, 88–95. https://doi.org/10.1016/j.isatra.2012.09.008

Sharma, D., Mishra, S., (2020). Disturbance-Observer-Based Frequency Regulation Scheme for Low-Inertia Microgrid Systems. IEEE Syst. J. 14, 782–792. https://doi.org/10.1109/JSYST.2019.2901749

Singh, K., Arya, Y., (2023a). Correction to: Jaya-ITDF control strategy based frequency regulation of multi microgrid utilizing energy stored in high voltage direct current-link capacitors. Soft Comput. 27, 5971–5971. https://doi.org/10.1007/s00500-023-08044-9

Singh, K., Arya, Y., (2023b). Jaya-ITDF control strategy-based frequency regulation of multi-microgrid utilizing energy stored in high-voltage direct current-link capacitors. Soft Comput. 27, 5951–5970. https://doi.org/10.1007/s00500-023-07839-0

Youssef, A.-R., Mallah, M., Ali, A., Shaaban, M.F., Mohamed, E.E.M., (2023). Enhancement of Microgrid Frequency Stability Based on the Combined Power-to-Hydrogen-to-Power Technology under High Penetration Renewable Units. Energies 16, 3377. https://doi.org/10.3390/en16083377

Zaid, S.A., Bakeer, A., Magdy, G., Albalawi, H., Kassem, A.M., El-Shimy, M.E., AbdelMeguid, H., Manqarah, B., (2023). A New Intelligent Fractional-Order Load Frequency Control for Interconnected Modern Power Systems with Virtual Inertia Control. Fractal Fract. 7, 62. https://doi.org/10.3390/fractalfract7010062

Zhao, W., Zhang, Z., Wang, L., (2020). Manta ray foraging optimization: an effective bio-inspired optimizer for engineering applications. Eng. Appl. Artif. Intell. 87, 103300. https://doi.org/10.1016/j.engappai.2019.103300

Zhong, Z., Huo, H., Zhu, X., Cao, G., Ren, Y., (2008). Adaptive maximum power point tracking control of fuel cell power plants. J. Power Sources 176, 259–269. https://doi.org/10.1016/j.jpowsour.2007.10.080